

Sources, concentrations, and seasonal variations of VOC and aerosol particles in downtown Munich in 2023/24

Yanxia Li¹, Hengheng Zhang^{1,a}, Xuefeng Shi¹, Yaowei Li^{2,b}, Sophie Abou-Rizk², Jessica B. Smith², Zhaojin An^{2,c}, Adrian Wenzel³, Junwei Song⁴, Thomas Leisner^{1,5}, Frank Keutsch², Jia Chen³, and Harald Saathoff¹

¹Institute of Meteorology and Climate Research-Atmospheric Aerosol Research, Karlsruhe Institute of Technology, 76344 Eggenstein-Leopoldshafen, Germany

²Paulson School of Engineering and Applied Sciences, Harvard University, Cambridge, MA 02138, USA

³Environmental Sensing and Modeling, Technical University of Munich (TUM), Munich, Germany

⁴Irceylon, Universite Claude Bernard Lyon 1, CNRS, UMR 5256, Villeurbanne, 69100, France

⁵Institute of Environmental Physics, Heidelberg University, 69120 Heidelberg, Germany

^anow at: Research Institute for Applied Mechanics, Kyushu University, Fukuoka, Japan

^bnow at: Department of Earth, Atmospheric, and Planetary Sciences, Massachusetts Institute of Technology, Cambridge, MA 02139, USA

^cnow at: School of Environment, Tsinghua University, 10084, Beijing China

Corresponding authors: Yanxia Li (yanxia.li@kit.edu) and Harald Saathoff (Harald.Saathoff@kit.edu)

Abstract. ~~Only a little~~ is known about molecular composition and sources of air pollution in Germany's third largest city, Munich. Therefore, we investigated sources, concentrations, and seasonal variations of volatile organic compounds (VOC), semi-volatile organic aerosol (SVOA), and organic aerosol (OA) in an urban street canyon in Munich utilizing online mass spectrometry and positive matrix factorization (PMF). Organic aerosol concentrations were higher in summer ($4.3 \pm 2.9 \mu\text{g m}^{-3}$) than late winter ($3.3 \pm 1.7 \mu\text{g m}^{-3}$), ~~consistent with due~~ ~~to~~ enhanced photochemical reactions, while nitrate exhibited the opposite trend with elevated concentrations in winter ($4.5 \pm 3.2 \mu\text{g m}^{-3}$) compared to summer ($0.3 \pm 0.2 \mu\text{g m}^{-3}$). During summer heat, photochemistry ~~is~~ ~~associated with the formation of~~ ~~generates~~ low-volatile oxygenated OA ($33 \pm 20\%$), while aged biomass burning organic aerosol (BBOA) ($25 \pm 21\%$) ~~associated with from~~ barbecue activities and biogenic OA ($22 \pm 14\%$) ~~linked to from~~ nocturnal monoterpene chemistry further shape aerosol composition. The colder seasons are characterized by combustion-derived aerosols (Winter: fresh BBOA $13 \pm 9\%$, aged $36 \pm 12\%$; Spring: fresh $27 \pm 17\%$, aged $37 \pm 19\%$), whose dynamics are driven mainly by anthropogenic activity patterns. Traffic contributed at this urban kerbside ~~relatively surprisingly~~ little to aerosol mass (5-9 %) but more to VOC (22-35%). Our findings point to ~~potential strategies efficient ways~~ to improve air quality e.g. by reducing monoterpene emissions by urban vegetation management as well as reducing biomass burning including barbecue emissions, ~~which are attributed to a substantial fraction a major source~~ of aerosol particles and precursor gases of secondary organic aerosol throughout the seasons.

1. Introduction

Volatile organic compounds (VOC) and organic aerosols (OA) are major components of urban air pollution, contributing to the formation of secondary pollutants like ozone and secondary organic aerosol (SOA), which pose significant risks to air quality, climate, and human health (Wu et al., 2020; Nault et al., 2021; Ipcc, 2023). Moreover, different weather conditions and seasons influence the dispersion, deposition, and transformation of

40 these pollutants (Crippa et al., 2013; Debevec et al., 2021; Stirnberg et al., 2021). Identifying SOA sources is
41 crucial for reducing complex observational datasets to key real-world contributors, enabling timely air quality
42 management, policy evaluation, and accurate air pollution forecasting (Chen et al., 2022a). However, pinpointing
43 the sources of SOA is particularly challenging due to its composition as a highly complex mixture of largely
44 unidentified compounds, coupled with the complicated and multistep transformation processes of VOC into SOA
45 (Daellenbach et al., 2019).

46 The high-resolution time-of-flight Aerodyne aerosol mass spectrometer (HR-TOF-AMS, [Aerodyne Research Inc.,
47 Billerica, MA, USA](#)) ~~quipped with a PM_{2.5} aerodynamic lens~~ is ~~commonly~~ used for the online characterization of
48 non-refractory PM_{2.5}. ~~AMS datasets combined with p~~Positive matrix factorization (PMF) analysis ~~of AMS
49 datasets~~ can quantitatively ~~identify-resolve~~ major primary organic aerosol (POA) sources, including traffic-related
50 hydrocarbon-like organic aerosol (HOA) and biomass burning organic aerosol (BBOA) (Chakraborty et al., 2017;
51 Lalchandani et al., 2021). However, AMS datasets cannot specify sources for secondary organic aerosol (SOA)
52 due to significant fragmentation from thermal volatilization (~600°C) and harsh electron impact ionization (~70
53 eV) (Qi et al., 2020; Kumar et al., 2022). Additionally, without information on VOC as SOA precursors, it is
54 difficult to attribute SOA factors (e.g., semi-volatile oxygenated OA (SV-OOA) and low-volatility oxygenated
55 OA (LV-OOA)) to specific sources or formation mechanisms using AMS-PMF analysis (Song et al., 2024).
56 Proton transfer reaction time-of-flight mass spectrometry (PTR-TOF-MS) is a useful tool to identify the sources
57 of VOC and oxygenated VOC (OVOC), and in elucidating their contributions to the SOA formation (Wang et al.,
58 2020a; Pfannerstill et al., 2019). Furthermore, the CHARON-PTR-MS (Chemical Analysis of Aerosol Online
59 Particle Inlet coupled to a PTR-TOF-MS) is a continuous measurement technique capable of [providing molecular-
60 level chemical characterization and time-resolved quantification of semi-volatile organic aerosol
61 components](#)~~qualitatively and quantitatively detecting semi-volatile organic aerosol particles~~ (Eichler et al., 2015;
62 Muller et al., 2017; Piel et al., 2019). CHARON-PTR-MS enhances the detection of detailed SOA chemical
63 composition data by minimizing thermal decomposition and ionization-induced fragmentation [compared to AMS
64 employing high-temperature vaporization and electron-impact ionization,](#) ~~providing more information on
65 identifying SOA sources compared to AMS~~ (Gkatzelis et al., 2018b; Leglise et al., 2019). [This is achieved through
66 lower thermal stress during particle evaporation at reduced pressure and softer chemical ionization via proton-
67 transfer reactions, which better preserves molecular information.](#)

68 Huang et al. (2019) found that in the city of Stuttgart (southwest Germany) SOA from VOC oxidation dominated
69 the organic aerosol burden, with primary sources like traffic contributing less, while residential wood burning
70 became particularly important during winter in residential areas. A study in ~~the downtown-of-the-city-of~~ Karlsruhe
71 (southwest Germany) demonstrated that secondary oxygenated OA comprised over 60-75% of total OA
72 throughout the year, with primary traffic-related OA showing seasonal variations and wood combustion becoming
73 more significant during cold periods under stagnant meteorological conditions (Song et al., 2022). A Europe-wide
74 analysis revealed that oxygenated OA (secondary formation) accounted for an average of 71% of submicron OA
75 mass across 22 sites, with solid fuel/biomass burning contributing 16% and primary urban sources (traffic,
76 cooking) typically less than 10-15% (Chen et al., 2022b). These findings underscore the necessity for site-specific
77 OA and VOC source apportionment studies in major European cities such as Munich in southern Germany ~~-, while
78 Although~~ secondary formation processes consistently dominate regional OA burdens, the underlying VOC
79 precursors, and primary emission contributions exhibit substantial spatial and temporal variability.

80 Munich, the capital of Bavaria, Germany, is a major cultural and economic center with a population of 1.5 million
81 as of 2023, making it the third-largest city in Germany. It has a population density of 4,700 people per square
82 kilometers (München, 2023). Despite significant progress in air quality regulations, Munich still struggles with
83 aerosol pollution. Identifying the sources of VOC and particulate matter is crucial for improving air quality in
84 Munich. However, there have been only a limited number of studies characterizing aerosols in Munich. Schnelle-
85 Kreis J. et al. (2001) collected filters from three traffic-dominated sites and one additional site located on the
86 northern outskirts of Munich, approximately 1 km from the city center, between 1996 and 1998. Using HPLC
87 analysis, they found that 40% of polycyclic aromatic hydrocarbons (PAHs) were associated with fine particles.
88 Schäfer et al. (2011) monitored air pollution across Munich and its outskirts, employing long-term as well as
89 campaign-based monitoring stations from LfU (Bayerisches Landesamt Für Umwelt), Meteorological Institute
90 of the Ludwig-Maximilians-University Munich (MIM), and IMK-IFU (e.g., Maisach) covering traffic-related
91 (e.g., Lothstraße, Stachus, Luise-KiesselbachPlatz), urban (MIM), and suburban (Johanneskirchen) sites, during
92 campaigns in late spring (10th-30th May 2003) and winter (27th November-15th December 2003). They found
93 higher particle mass concentrations at the urban site compared to rural areas, especially in winter, with no
94 significant differences in major ionic composition between the sites (Schäfer et al., 2011). Qadir et al. (2013)
95 identified traffic, cooking, solid fuel combustion, and mixed aerosols (from tobacco smoke, cooking, and wood
96 combustion) as the primary sources of aerosols at Lothstraße in Munich during the winter periods of October 2006
97 to February 2007 and October 2009 to February 2010. Schnell (2014) identified biomass burning aerosol as the
98 dominant aerosol type at the rural site of Maisach and the urban site of MIM during the winter seasons from 2007
99 to 2010. Recently, a study on aerosol emissions from Munich Airport showed its impact in the outskirts of Munich,
100 especially for ultrafine particles (UFPs) (Seidler et al., 2024). Despite these previous studies, we still have limited
101 understanding of the main sources of VOC and OA through concurrent online measurements, their typical
102 concentration levels across seasons, and their seasonal variations in molecular composition in Munich. It remains
103 unclear how much anthropogenic and biogenic sources contribute to ~~air pollution~~organic aerosol in Munich and
104 what is the fraction of biomass burning aerosol originates from residential wood combustion versus barbecue
105 activities~~wood combustion vs. barbecue for biomass burning aerosol~~. Therefore, we examined in this study the
106 seasonal variability of OA and VOC chemical composition at a molecular level in a street canyon
107 (Theresienstrasse 39) in downtown Munich, aiming to elucidate the contribution of different sources to major
108 VOC, SVOA, and total OA concentrations. The PM_{2.5} concentrations at the Theresienstrasse were measured using
109 a FIDAS 200 optical particle spectrometer (Palas GmbH, Germany) and are comparable to those observed at the
110 regulatory monitoring station Munich/Stachus of LfU. For 2023, the annual average PM_{2.5} concentration at the
111 reference station was $9.3 \pm 6.2 \mu\text{g m}^{-3}$, with August showing $8.7 \pm 5.7 \mu\text{g m}^{-3}$, compared to our measured value
112 of $6.7 \pm 3.7 \mu\text{g m}^{-3}$. In 2024, the annual average at the reference station was $8.7 \pm 6.6 \mu\text{g m}^{-3}$, with March averaging
113 $9.0 \pm 9.9 \mu\text{g m}^{-3}$, while our March measurements yielded $8.7 \pm 9.2 \mu\text{g m}^{-3}$. Both measurement periods
114 demonstrated strong correlations ($R=0.8$) (Figure S1). The close agreement between our measurements and the
115 official monitoring data, combined with the high correlation coefficients, validates the representativeness of our
116 sampling location for characterizing the urban downtown atmosphere in Munich. Please note that this work is
117 linked to the recently established low-cost sensor network in downtown Munich, monitoring especially O₃, NO₂,
118 and PM_{2.5} (Wenzel et al., 2025). For our dedicated source apportionment, we conduct separate statistical analyses

119 on VOC from PTR-TOF-MS, SVOA from CHARON-PTR-MS, and OA from HR-TOF-AMS to identify the
120 sources of VOC, SVOA, and OA from their chemical fingerprints.

121 2. Methodology

122 2.1 Measurement location

123 Field observations were conducted during three meteorological periods distinct seasons: summer (3rd-29th August
124 2023), late winter (1st-8th March 2024), and spring (9th-27th March 2024). The separation between winter and
125 spring periods was based on observed transitions in ambient temperature and chemical composition, including
126 systematic changes in organic aerosol and nitrate concentrations observed in the time series (Figure 1d and Figure
127 2), indicating a shift from colder, nitrate-favored conditions to warmer conditions associated with enhanced
128 photochemical activity, ambient temperature trends and nitrate concentrations. Spring conditions were
129 characterized by higher solar radiation and an increased relative contribution of organic aerosol (Figure 1d and
130 Figure 2), reflecting stronger photochemical production. These periods therefore represent meteorologically and
131 chemically distinct regimes rather than strict calendar-based seasonal classifications. The sampling site (11°57'E,
132 48°15'N) was located on a parking lot next to a 30 m tall building of the Ludwigs-Maximilians-University (LMU)
133 of Munich in a street canyon of Theresienstrasse 39 (Figure S2). The elevation on street level at this location is
134 520 m a.s.l. The street has several restaurants, apartment buildings, museums, university workshops, laboratories,
135 and substantial vehicular traffic. The wind direction at the site in the street canyon predominantly originates from
136 the south and southeast due to a vortex due to upwind or lee side of the LMU building. At the rooftop of the 30-
137 meter LMU building, it mainly came from the west and east. Wind speed and direction exhibit minimal variation
138 for the measurement periods (Figure S2).

139 2.2 Instrumentation

140 An overview of all instruments used in this campaign to characterize aerosol particles, trace gases, and
141 meteorological parameters is provided in Table S1. The major instruments used are described in more detail below.

142 2.2.1 CHARON-PTR-TOF-MS

143 A proton-transfer-reaction time-of-flight mass spectrometer (PTR-ToF-MS 4000X2, Ionicon Analytik GmbH),
144 equipped with a particle inlet (Chemical Analysis of aeRosol ONline, CHARON), was utilized to measure VOC
145 in the gas phase and semi-volatile compounds in the particle phase. The PTR-ToF-MS 4000X2 employed here
146 has an ion funnel, which reduces ion loss and enhances sensitivity (Pugliese et al., 2020). The CHARON inlet
147 integrates a gas-phase denuder, an aerodynamic lens with an inertial sampler, and a thermo-desorption unit, all
148 coupled to a PTR-TOF-MS. The gas-phase denuder removes gas-phase analytes, while the aerodynamic lens
149 focuses the aerosol particles. The inertial sampler then concentrates the particle-enriched sample flow. Finally,
150 the particles enter a thermal desorption unit where they are volatilized before being detected by PTR-MS. The
151 inlet system demonstrated a particle enrichment factor of 18 ± 2 (Figure S3), as discussed in detail in our previous
152 study (Song et al., 2024). The vaporizer (TDU) was operated at 150 °C and 7-8 mbar absolute pressure. The
153 CHARON inlet was described in detail elsewhere (Eichler et al., 2015; Muller et al., 2017; Gkatzelis et al., 2018a;
154 Gkatzelis et al., 2018b).

155 In this campaign, the CHARON-PTR-MS automatically switched between gas and particle phase measurements.
156 The sequence was: 5 minutes of high-efficiency particulate air (HEPA) filter measurement for particle background,
157 10 minutes of particle-phase measurement, 3 minutes transition, 10 minutes of gas-phase VOC measurement, and
158 another 2 minutes transition. The PTR drift tube was kept at 2.7 mbar, 470 V, and 100 °C, with the ion funnel at
159 45 V. These settings correspond to an electric field (E) to gas molecule number density (N) ratio of ~100 Td for
160 VOC measurement. For particle measurement, the PTR was automatically adjusted to 60 Td.
161 During gas-phase measurement, ambient air was sampled continuously from a 2 m PFA tube (4 mm inner diameter)
162 at 8 L/min, with 40-100 mL/min directed to the PTR-ToF-MS through a polyetheretherketone (PEEK) tubing at
163 80°C. The instrumental background was determined weekly at noon by introducing pure dry nitrogen (N₂,
164 99.9999%) into the inlet for 5–15 min to exclude ambient air and quantify the instrumental baseline (Figure S4).
165 ~~The gas background was manually measured weekly using pure nitrogen for 5–15 minutes.~~ For particle-phase
166 measurement, ambient particles were sampled with a PM_{2.5} inlet (Comde Dendra) through a vertical
167 electropolished 3.45 m stainless-steel tube (12 mm inner diameter) at 16.7 L/min, with 550 mL/min directed to
168 the CHARON inlet. Particle background was automatically determined using the HEPA filter.

169 Gas calibrations were performed at the beginning, middle, and end of each campaign periods using a gas cylinder
170 (Ionicon Analytik GmbH) with 15 VOC, including toluene, trimethylbenzene, xylene, alpha-pinene, acetone,
171 acetonitrile, benzene, and isoprene (accuracy 5% at ~1000 ppb). The sensitivity ranged from ~1000 to 4000
172 cps/ppb for different compounds across different seasonal calibration periods (Figure S4S5). Raw data from
173 CHARON-PTR-MS were processed using IONICON Data Analyzer software (IDA 2.2.0) following Müller et al.
174 (2013), Lannuque et al. (2023), and Peron et al. (2024). The CHARON inlet enrichment factor was determined
175 via external calibration with size-selected (DMA, TSI) ammonium nitrate particles (100-500 nm) measured by a
176 condensation particle counter (CPC, TSI).

177 2.2.2 HR-TOF-AMS

178 A high-resolution time-of-flight Aerosol Mass Spectrometer (HR-ToF-AMS) (Aerodyne Research Inc.),
179 equipped with a PM_{2.5} aerodynamic lens, was used to measure non-refractory PM_{2.5} (NR-PM_{2.5}) components,
180 including organic aerosol, nitrate, sulfate, ammonium, and chloride, with a time resolution of 1 minute (Peter F.
181 Decarlo et al., 2006; Canagaratna et al., 2007; Williams et al., 2013). The operation and calibration procedures of
182 the AMS are detailed in our previous publications (Huang et al., 2019; Song et al., 2022). The instrument's
183 capability to provide high-resolution mass spectra enables detailed chemical composition analysis of aerosol
184 particles in real time. Briefly, ambient air was sampled through a PM_{2.5} inlet (flow rate of 1 m³ h⁻¹) that was shared
185 with the CHARON system via a 3.45 m stainless-steel tube. A subset of this flow was then directed to the HR-
186 ToF-AMS at a flow rate of 84 cm³ min⁻¹. The aerosol particles were focused into a narrow beam by a PM_{2.5}
187 aerodynamic lens, which effectively transmits particles with vacuum aerodynamic diameters (d_{va}) ranging from
188 ~70 to ~2500 nm. The particles were subsequently heated by a vaporizer at 600°C, causing the non-refractory
189 components to volatilize. The volatilized particles were then ionized by electron impact at 70 eV, which is a
190 standard method for ionizing organic and inorganic compounds, ensuring fragmentation patterns that are well-
191 characterized and suitable for identification. The AMS was calibrated using ~~~300 nm~~-dried ammonium nitrate
192 aerosol particles with sizes of 100-500 nm to optimize-determine ionization efficiency and instrument response.
193 lens transmission (70-500 nm) and ionization efficiency. Calibration particles were size-selected using a DMA.

194 ~~and signal stability was verified prior to and during each measurement period. with DMA selection and signal~~
195 ~~validation. The calibrations were done before and each measurement period.~~ Data from the AMS were processed
196 and analyzed using the SQUIRREL 1.65G and PIKA 1.25G software packages. To address the issue of particle
197 bounce losses, a chemical-composition-based collection efficiency (CE) of approximately 0.5 was applied to
198 calculate the particle mass concentrations (Docherty et al., 2011; Middlebrook et al., 2012). For the elemental
199 analysis of organic aerosol (OA), including the hydrogen-to-carbon ratio (H: C) and the oxygen-to-carbon ratio
200 (O: C), we utilized the improved ambient method (Allison C. Aiken et al., 2008; Canagaratna et al., 2015).

201 **2.2.3 Other Instruments**

202 The mass concentrations of PM_{2.5} and PM₁₀ and particle size distributions (0.2-18 μm) were determined using an
203 optical particle counter (Fidas200, Palas). Particle number concentrations (> 2.5 nm) were monitored using a
204 water-based condensation particle counter (Model 3789, TSI Inc.) and a butanol-based condensation particle
205 counter CPC3776 (TSI Inc., USA). Particle number size distributions ranging from 10 to 410 nm were measured
206 using a nanoparticle sizer (Nanoscan 3910; TSI Inc.) at time resolution of 1 min in winter, and distributions
207 ranging from 13.6 to 763.5 nm were measured using a scanning mobility particle sizer (SMPS; DMA 3081; TSI
208 Inc.) at a time resolution of 7 min in Summer. Equivalent black carbon (eBC) levels were monitored with an
209 aethalometer (AE33, Magee Scientific) at a 1-minute resolution. Ammonia (NH₃) concentrations were measured
210 via cavity ring-down spectroscopy (G2103, Picarro Inc.). The gas was sampled via a Teflon tube (4 mm i.d.; 3.1s
211 residence time). Ozone (O₃) and nitrogen dioxide (NO₂) concentrations were tracked using the O₃41M and
212 AS32M gas analyzers (both from Environment S.A.), respectively. Meteorological parameters such as
213 temperature, relative humidity, wind speed and direction, global radiation, and precipitation were recorded with a
214 compact weather sensor (WS700, Lufft) installed on the container roof. Additional meteorological data was
215 measured by the Institute of Meteorology of the LMU on top of the institute at about 30 m above ground level
216 (<https://www.meteo.physik.uni-muenchen.de/request-beta/>). The vertical aerosol distribution was assessed using
217 a scanning aerosol Lidar (Rametris Inc., Type: LR111-ESS-D200, named KASCAL). Fiber laser-induced
218 fluorescence (FILIF) detects formaldehyde (HCHO) by exciting molecules at 353 nm and measuring fluorescence
219 above 370 nm. The technique alternates between on-peak and off-peak laser frequencies to determine HCHO
220 concentration with high specificity. Calibrated against FTIR standards, FILIF achieves ± 27 pptv precision (10-
221 15% accuracy) at 10 Hz sampling frequency, unaffected by humidity. All the information could be found in
222 previous studies (Ye et al., 2021). Unless otherwise specified, all measured values are reported as mean ± standard
223 deviation. Please note that this work is linked to the recently established low-cost sensor network in downtown
224 Munich, monitoring especially O₃, NO₂ and PM_{2.5} (Chen, 2025). This included frequent comparison
225 measurements between reference instruments on a bicycle platform, the instruments in our container, a LfU
226 regulatory monitoring station, and the low-cost sensor network in downtown Munich. Back trajectories were
227 calculated using the Hybrid Single-Particle Lagrangian Integrated Trajectory (HYSPPLIT) model (Stein et al., 2015)
228 at 500 m altitude with 72-hour backward duration to identify potential source regions and transport pathways
229 influencing air quality at the measurement site.

230 2.2.4 PMF analysis

231 The PMF receptor model is a bilinear algorithm that separates air pollutant time series into sources characterized
232 by factor profiles, time series, and residuals (Paatero and Tapper, 1994; Paatero, 1999). It is widely used to identify
233 particle and VOC sources (Kim et al., 2004; Reyes-Villegas et al., 2016; Huang et al., 2018; Gkatzelis et al., 2021).
234 PMF has also been applied to inorganic aerosol components, elemental composition of particulate matter (PM),
235 VOC, PAHs, black carbon, and size-resolved particle data, showing its versatility as a receptor model across
236 various pollutant types (Äijälä et al., 2019). PMF has been used for analyzing high-time-resolution elemental data
237 in PM_{2.5} and PM₁₀ to identify urban and industrial sources and to separate fine and coarse particle sources
238 (Reizer et al., 2021). Reviews and guidelines from European air quality agencies explicitly mention the use of
239 PMF applied to particle mass, ions, metals, and gaseous species (like VOC and PAHs) in addition to OA for
240 comprehensive source apportionment studies (Belis et al., 2013). In summary, PMF receptor modeling is broadly
241 used and suitable for source apportionment of multi-pollutant data sets.

242 To investigate the sources of VOC, SVOA, and OA, positive matrix factorization (PMF) was applied separately
243 to (i) VOC mass spectra measured by PTR-MS, (ii) semi-volatile aerosol species measured by CHARON-PTR-
244 MS, and (iii) OA measured by HR-TOF-AMS. we conducted PMF analysis on VOC mass spectra from PTR-MS,
245 semi-volatile aerosol species measured by CHARON PTR MS, and OA measured by HR TOF AMS,
246 respectively. PMF analyses were conducted independently for each dataset and measurement campaign rather
247 than using a combined dataset. Separate analyses were chosen because the campaigns were performed in different
248 seasons under substantially different atmospheric conditions and instrument states. PMF assumes temporally
249 stationary factor profiles and comparable uncertainty structures within a dataset; these assumptions are not
250 fulfilled when combining measurements across seasons with distinct source contributions and atmospheric
251 processing regimes. In addition, VOC and SVOA datasets were analyzed separately because they represent
252 chemically and physically distinct phases with different atmospheric processing timescales, variability patterns,
253 and measurement uncertainty structures. Combining these datasets in a single PMF analysis would violate the
254 assumption of consistent covariance structure and could lead to mixed or non-interpretable factors. Diagnostic
255 evaluations supporting solution stability and factor selection for each dataset are provided in the Supplement
256 (Figures S8-S20). The PMF analysis in this study incorporated both VOC and SVOA as distinct input matrices.

257 For VOC-PMF, inputs were derived from PTR-TOF-MS data following the methodology of Song et al. (2024),
258 involving comprehensive preprocessing including mass spectral deconvolution, background subtraction, and error
259 matrix calculation where uncertainties were determined as $[(0.1 \times \text{concentration})^2 + (0.5 \times \text{LOD})^2]^{1/2}$ (Kajos et al.,
260 2015). SVOA-PMF inputs were obtained through two complementary measurement modes: HEPA-filtered air
261 samples (representing background signals) and direct atmospheric sampling (Dir) capturing real-time conditions,
262 with ions (primarily C_xH_y^+ , $\text{C}_x\text{H}_y\text{O}_z^+$, and $\text{C}_x\text{H}_y\text{O}_z\text{N}_n^+$). Both datasets underwent rigorous quality control
263 procedures. Low-molecular-weight species ($m/z \leq 60$) were excluded to eliminate potential interferences from
264 fragments and common atmospheric gases that may not be representative of specific emission sources (Zhang et
265 al., 2011). Additionally, compounds with $\geq 20\%$ missing data points were removed to ensure statistical robustness
266 in the PMF analysis, following established protocols for PMF data preparation (Ulbrich et al., 2009; Zhang et al.,
267 2011). The analyses were initially processed using SoFi Pro 9.0 (Datalystica Ltd.) for exploratory factor analysis
268 and data visualization. The source apportionment of organic aerosols (m/z 12-120) was then conducted through

269 unconstrained AMS-PMF analysis using the PMF Evaluation Tool (v3.08C) within IGOR Pro (v8.04), which
270 maintains legacy algorithms specifically optimized for AMS datasets, particularly for handling nonlinear m/z
271 signal-uncertainty relationships in typical AMS operating conditions.

272 The final number of factors for each dataset was selected based on a combination of diagnostic criteria, including
273 the evolution of Q/Q_{exp} values, inspection of scaled residual distributions, physical interpretability of factor
274 profiles, and temporal behavior. Physical interpretability was evaluated using dominant marker compounds in
275 each factor mass spectrum together with their temporal patterns, allowing source attribution based on established
276 source signatures (e.g., traffic-related factors identified by toluene/xylene dominance and rush-hour diurnal peaks).
277 Solutions with increasing factor numbers were examined to identify the point beyond which additional factors
278 primarily resulted in factor splitting without meaningful improvement in residual structure. Detailed diagnostics,
279 including Q/Q_{exp} evolution, residual analysis, F_{peak} sensitivity tests, and correlations with characteristic
280 compound markers and diurnal patterns, are provided in the Supplement (Section S3.2, Figures S7 – S19, Table
281 S4 – S9).

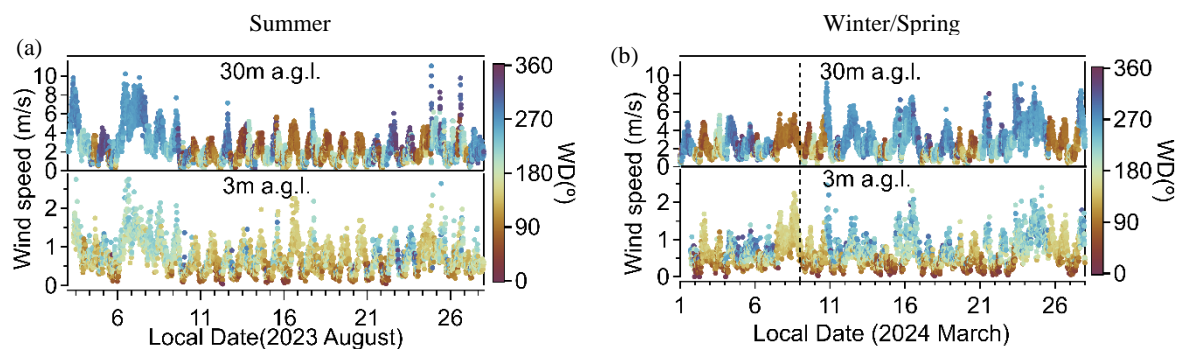
282 3. Results and discussion

283 In the first section, we give an overview of the meteorological conditions during the two measurement campaigns
284 and the main characteristics of the observed evolution of aerosol particles and trace gases. The second section will
285 discuss the major sources of aerosol particles and trace gases. In the third section, we focus on strong biomass
286 burning events.

287 3.1 Overview of observations during summer and wintertime

288 3.1.1 Overview of meteorological and particle observations

289 The summer period was characterized by frequent sunny weather with moderate to high temperatures and
290 significant precipitation events mainly at the beginning and end of the summer campaign. The late winter/spring
291 period shows typical winter conditions until March 8th, according to temperature, precipitation followed by more
292 spring-like conditions thereafter.



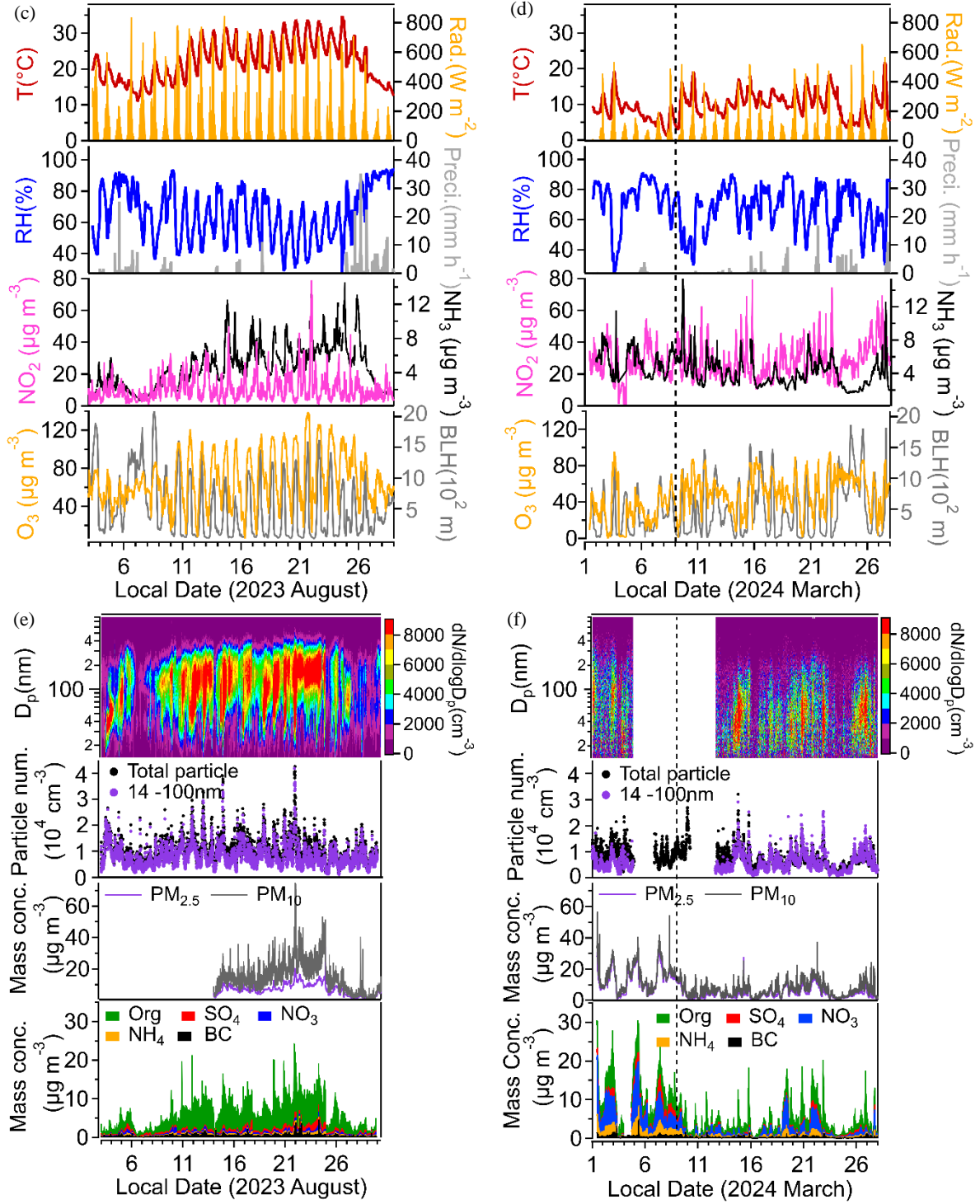


Figure 1: Time series of wind speed & direction 3m (above ground level) and 30 m (above ground level) in summer (a) and winter (b); temperature (T); global radiation (Ra); relative humidity (RH); precipitation; NO_2 ; NH_3 ; O_3 and boundary layer height (BLH*) in summer (c) and winter (d); Particle number size distributions; particle number of total and below 100nm ultrafine particles; $\text{PM}_{2.5}$ and PM_{10} mass concentrations; Organic aerosol (OA), sulfate, nitrate, and ammonium; Equivalent black Carbon (eBC) in summer (e) and (f) in winter; #All data plotted except the wind data were measured at the container roof. *Please note that the BLH data refer to ERA5 reanalysis data (Guo et al., 2024), **which represent large-scale boundary layer conditions and may not fully capture street-canyon ventilation or local turbulence effects. The vertical dotted line marks the transition between the late-winter and early-spring periods, defined based on observed changes in temperature, solar radiation, and aerosol chemical composition.**

293 Wind measurements at 3 m and 30 m above ground (Figure 1a-b) revealed consistent vertical gradients across all
294 seasons, with average speeds of 0.7 ± 0.4 and 2.6 ± 1.4 m s⁻¹, respectively. Meteorological conditions varied
295 significantly between seasons (Figure 1c-d), creating distinct chemical environments. The higher summer
296 temperatures (21.9 ± 5.8 °C) promoted enhanced biogenic emissions and photochemical activity, while lower
297 winter temperatures (8.4 ± 3.0 °C) favored primary pollutant accumulation. Relative humidity and total
298 precipitation showed minimal seasonal variation. NO₂ concentrations were 2.5-2.8 times higher in winter/spring
299 (26.1 ± 9.9 / 28.4 ± 10.8 µg m⁻³) than summer (10.2 ± 7.7 µg m⁻³) due to increased heating emissions and reduced
300 photolysis under shallow boundary layers (339 ± 298 m / 510 ± 477 m vs 516 ± 453 m, variability). The BLH
301 values are derived from ERA5 reanalysis and represent regional-scale atmospheric mixing. They do not resolve
302 street-canyon ventilation. In a street canyon, buildings can limit horizontal and vertical dispersion, especially
303 under stable winter conditions. Therefore, pollutant accumulation at the measurement site may be stronger than
304 suggested by ERA5 BLH alone. This limitation is particularly relevant for reactive pollutants such as NO₂. In
305 addition to dispersion, NO₂ is strongly influenced by local traffic emissions and rapid photochemical processes
306 (e.g., photolysis and O₃ titration). As a result, short-term variations in NO₂ may reflect a combination of street-
307 canyon trapping, advection, and chemical transformation. This can differ from more inert traffic-related species
308 such as BC, which are primarily governed by physical mixing. The ERA5 BLH should therefore be interpreted as
309 an indicator of large-scale mixing conditions rather than street-level ventilation. The LfU station showed similar
310 winter (27.2 ± 9.2 µg m⁻³) and early spring (27.8 ± 9.2 µg m⁻³) mean concentrations to Theresienstrasse, but
311 exhibited weak temporal correlation, reflecting the strong spatial variability of NO₂. Notably, summer NO₂ at LfU
312 (23.4 ± 10.1 µg m⁻³) was 2.3 times higher than Theresienstrasse, yet temporal correlation improved substantially
313 ($R = 0.5$) in Figure S5S6. This seasonal pattern suggests that summer's higher boundary layer enhanced vertical
314 mixing and local photochemical reactions, increasing spatial differences in mean NO₂ levels. However, stronger
315 synchronized daily photochemical cycles improved temporal agreement between the two sites. The diurnal
316 evolution of NO₂, O₃, and BLH reveals seasonally distinct coupling between photochemical processing and
317 boundary-layer mixing (Figure S7). During summer, increasing BLH coincides with decreasing NO₂
318 concentrations and enhanced daytime O₃ formation, indicating efficient vertical mixing and active photochemical
319 processing. Spring exhibits intermediate behavior, whereas winter shows weaker BLH development and
320 persistently elevated NO₂ levels consistent with reduced photolysis and limited dispersion. Gaseous NH₃ showed
321 elevated concentrations across all seasons, with winter (5.4 ± 1.5 µg m⁻³) and spring (4.0 ± 1.8 µg m⁻³) levels
322 comparable to summer values (4.8 ± 2.6 µg m⁻³). O₃ concentrations at Theresienstrasse exhibited strong seasonal
323 variation, with highest levels in summer (67.1 ± 26.6 µg m⁻³), followed by early spring (52.2 ± 19.3 µg m⁻³), and
324 lowest in late winter (32.4 ± 20.2 µg m⁻³). The LfU station showed similar seasonal patterns (summer: 59.3 ± 25.5
325 µg m⁻³; late winter: 30.8 ± 17.3 µg m⁻³; early spring: 45.9 ± 17.2 µg m⁻³) with strong temporal correlations ($R =$
326 0.8 in August 2023; $R = 0.7$ in March 2024) in Figure S5S6, indicating consistent O₃ behavior across both sites
327 driven by regional photochemical processes.

328 Particle size distributions revealed contrasting seasonal patterns driven by different formation mechanisms
329 (Figures 1e-f). Summer showed the highest total particle number concentrations (10000 ± 5100 cm⁻³) with a
330 substantial variability dominated by ultrafine particles (< 100 nm: $80.6 \pm 8.2\%$), indicating a strong contribution
331 of ultrafine particles during this period, enhanced new particle formation under intense photochemical conditions

332 ~~and elevated precursor concentrations.~~ Winter exhibited lower total number concentrations ($8900 \pm 3500 \text{ cm}^{-3}$)
 333 and a lower fraction of ultrafine particles ($33.6 \pm 10.1\%$), consistent with a greater relative contribution of aged
 334 and accumulation-mode particles under stable conditions,~~consistent with reduced photochemical activity and~~
 335 ~~primary emission dominance.~~ Spring showed intermediate behavior with high ultrafine fractions (89.7%) but
 336 lower absolute number concentrations. The seasonal PM mass concentrations showed opposite trends to the
 337 particle number concentrations: winter $\text{PM}_{2.5}$ peaked at $13.0 \pm 7.4 \mu\text{g m}^{-3}$ with nitrate as the dominant component
 338 due to low temperatures, shallow boundary layers and increased residential heating. In contrast, summer ($6.7 \pm$
 339 $3.7 \mu\text{g m}^{-3}$) and spring ($4.2 \pm 3.1 \mu\text{g m}^{-3}$) showed lower $\text{PM}_{2.5}$ levels dominated by organic aerosols, despite higher
 340 particle numbers, highlighting that ultrafine particles can dominate number concentrations in urban environments
 341 while contributing comparatively little to total particulate mass,~~suggesting predominance of freshly formed~~
 342 ~~ultrafine particles that contribute little to total mass.~~

343 Aerosol particle mass composition varies significantly by season, reflecting different formation mechanisms.
 344 Organic aerosol particles dominate in summer due to high photochemical activity (Figures 2), averaging 4.3 ± 2.9
 345 $\mu\text{g m}^{-3}$, higher than $3.3 \pm 1.7 \mu\text{g m}^{-3}$ in winter and $1.8 \pm 1.8 \mu\text{g m}^{-3}$ in spring. Nitrate is the main component in
 346 winter ($4.5 \pm 3.2 \mu\text{g m}^{-3}$) due to low temperatures favoring particle phase and increased heating emissions
 347 providing abundant NH_3 and NO_x precursors for ammonium nitrate formation. Nitrate concentrations drop
 348 significantly in spring ($1.0 \pm 1.3 \mu\text{g m}^{-3}$) and summer ($0.3 \pm 0.2 \mu\text{g m}^{-3}$) as rising temperatures shift the equilibrium
 349 toward the gas phase. Ammonium follows similar patterns, peaking in winter ($1.8 \pm 1.1 \mu\text{g m}^{-3}$) and remaining
 350 low in warmer seasons (spring: $0.4 \pm 0.4 \mu\text{g m}^{-3}$; summer: $0.3 \pm 0.2 \mu\text{g m}^{-3}$), consistent with reduced ammonium
 351 nitrate formation.

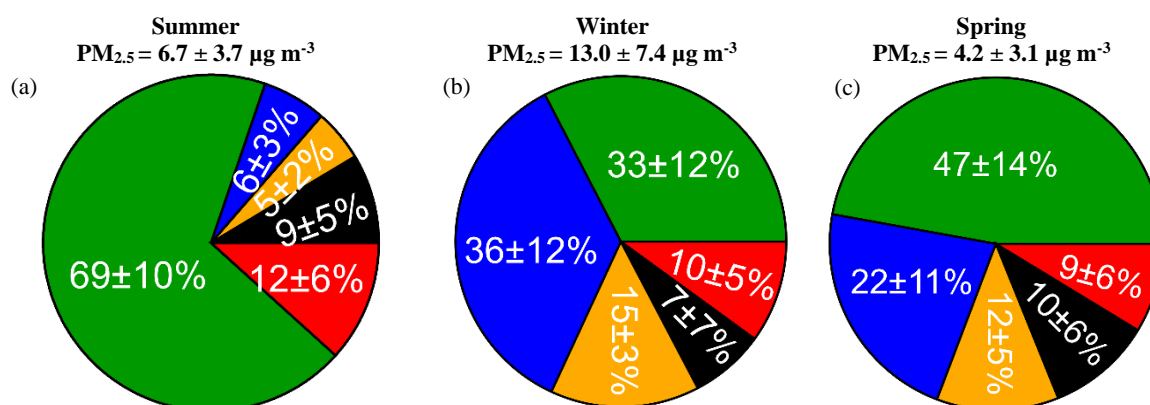


Figure 2: Average fractions of $\text{PM}_{2.5}$: OA (green), sulfate (red), nitrate (blue), ammonium (yellow) and eBC (black) in summer (a), (b) in winter (until March 8th) and (c) in spring based on AMS and Aethalometer measurements.

352 3.1.2 Diurnal behaviour of gaseous BVOC and BTEX

353 The average diurnal variations of key volatile organic compounds (VOC) are examined below, focusing on major
 354 biogenic and anthropogenic species, including BTEX—a group of aromatic hydrocarbons comprising benzene,
 355 toluene, ethylbenzene, and xylene. The VOC selected here comprise $32.3 \pm 13.1\%$ of all VOC detected in summer,
 356 $41.0 \pm 12.9\%$ in winter and $37.9 \pm 12.5\%$ in spring.

357 Figure 3 illustrates the diurnal variations of six VOC across three seasons, revealing distinct patterns tied to their
 358 sources and environmental influences. Isoprene and monoterpenes, both biogenic VOC, exhibit the highest mixing
 359 ratios in summer. However, Isoprene displays a bimodal pattern in summer and spring, with concentration peaks

360 during the morning and evening hours, suggesting a potential link to traffic activity during the morning and
 361 evening hours. This is consistent with direct measurements of isoprene in vehicle exhaust by Borbon et al. (2001).
 362 Additionally, fragmentation of higher-carbon aldehydes and cycloalkanes from anthropogenic sources may
 363 contribute to the signal of isoprene, further complicating source attribution in urban environments (Coggon et al.,
 364 2024b). Monoterpene exhibited early morning peaks in summer and spring, but was almost flat in winter. In
 365 contrast, their concentrations are minimal in winter due to suppressed biological activity. Anthropogenic VOC
 366 like benzene, toluene, xylene, and trimethylbenzene show different seasonal behaviors. Benzene peaks in winter,
 367 likely due to lower BLH and reduced dispersion, with dips at midday possibly from increased OH radical oxidation
 368 under sunlight. Toluene, xylene, and trimethylbenzene display notable spikes in spring, particularly during
 369 morning and evening hours, suggesting strong contributions from traffic emissions and industrial activities.

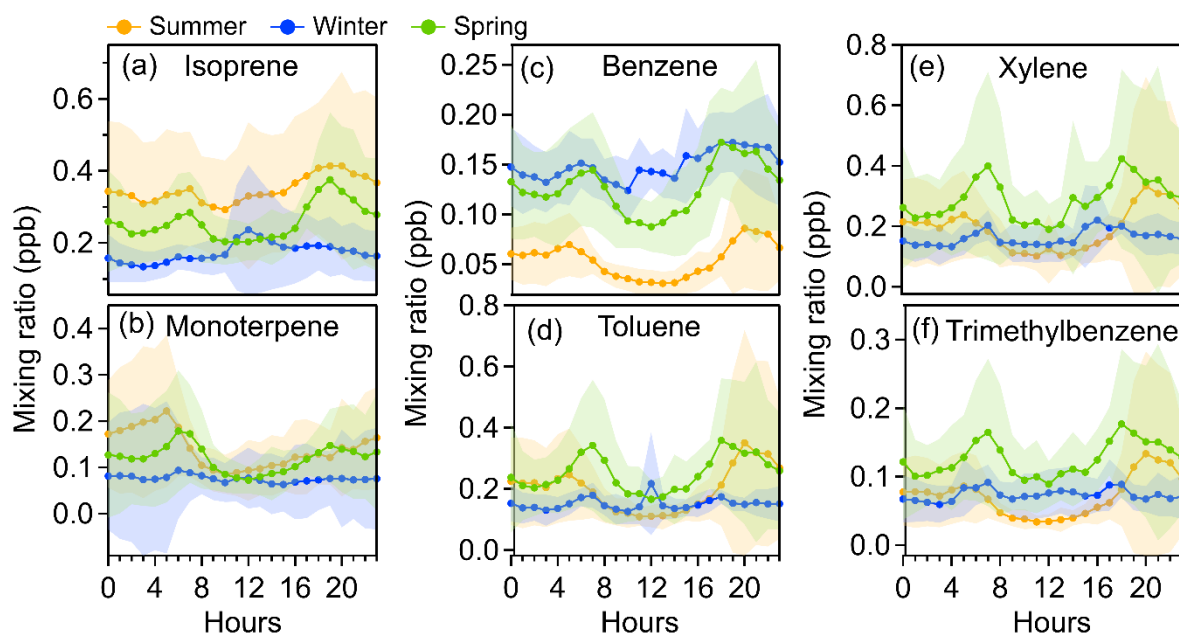


Figure 3: Diurnal behavior of (a) Isoprene, (b) Monoterpenes, (c) Benzene, (d) Toluene, (e) Xylene and (f) Trimethylbenzene in summer, winter and spring.

370 3.2 Sources of VOC and organic aerosol particles

371 In this section we use statistical (PMF) analysis of on-line mass spectra from VOC (PTR-MS) and semi-volatile
 372 organic aerosol particles (CHARON-PTR-MS) as well as organic aerosol particles (HR-TOF-AMS) to determine
 373 their major sources.

374 3.2.1 VOC sources in summer and winter

375 We included 117 VOC ions (Table S2) for PMF analysis in summer and 97 VOC ions (Table S3) in winter/spring.
 376 Ions with extremely high signal intensities that could disproportionately influence the PMF solution, as well as
 377 very low signal ions with minimal contribution, were excluded. The excluded high-abundance ions are common
 378 hydrocarbon and oxygenated VOC fragments, such as m/z 33.034 ($C_1H_5O^+$), 41.039 ($C_3H_5^+$), 43.054 ($C_3H_7^+$),
 379 45.034 ($C_2H_5O^+$), 57.070 ($C_4H_9^+$), and 59.049 ($C_3H_7O^+$), excluding abundant ions that could skew results and
 380 very low ion signals with minimal impact. Abundant These ions (e.g., fragments of alkanes or oxygenated VOC)
 381 were removed because their high concentrations may lead to over-representation of certain specific factors, while
 382 whereas low-signal ions were excluded to reduce noise interference (Song et al., 2024). The average VOC

383 molecules mixing ratio is 3.4 ± 1.0 ppb in summer, 2.1 ± 0.7 ppb in winter, and 3.4 ± 1.7 ppb in spring. This study
 384 thoroughly examined factor profiles, diurnal patterns, and correlations with tracers (Figure 4, S6-S8 and Table S4)
 385 for summer and for winter (Figures S7-S9, S108 and Table S5). Five factors were identified based on measured
 386 VOC as the optimal interpretable solutions for summer and winter, respectively.

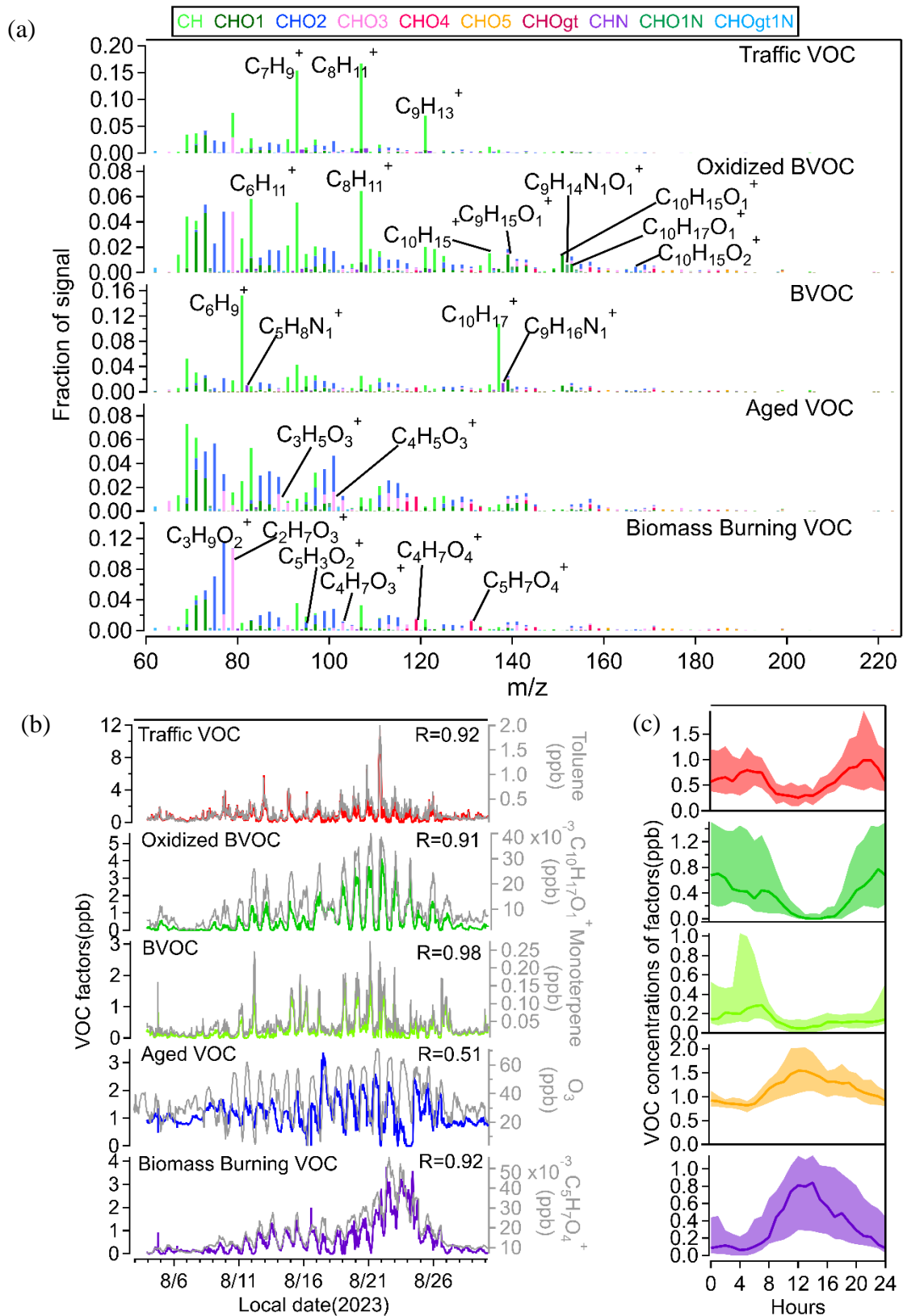


Figure 4 VOC source apportionment for summer time. (a) Normalized VOC factor mass spectra from PMF analysis and characteristic mass peaks in summer; (b) Time series of VOC factors including traffic, oxidized BVOC, BVOC, aged VOC, and biomass burning VOC; (c) Median diurnal variations in VOC factors during summer time

387 In summer, the first factor was characterized by high contributions and strong correlations with aromatic
388 hydrocarbon ions, such as $C_7H_9^+$ (m/z 93.07), $C_8H_{11}^+$ (m/z 107.086), and $C_9H_{13}^+$ (m/z 121.102). These compounds
389 correspond to toluene, xylenes, and C₉-aromatics, commonly used as vehicular emission markers (Squires et al.,
390 2020; Jain et al., 2022). We assigned it to traffic VOC. These ions show a correlation coefficient (R) of
391 approximately 0.9 with traffic emissions (Table S3). According to the diurnal profiles of traffic (Figure 4) in
392 summer, it shows distinct peaks during morning and evening hours.

393 The second factor was classified as weakly oxidized BVOC. It was identified by oxidation products of
394 monoterpenes, specifically $C_9H_{15}O_1^+$ myrcenol (m/z 139.112), $C_{10}H_{13}O_1^+$ carvone (m/z 149.097), weakly-oxidized
395 molecules of monoterpenes $C_{10}H_{15}O_1^+$ (m/z 151.112), $C_{10}H_{17}O_1^+$ (m/z 153.128) and $C_{10}H_{15}O_2^+$ (m/z 167.107) (Li
396 et al., 2020a). These ions show strong correlations with the Oxidized BVOC factor, with R values of 0.93, 0.93,
397 0.93, 0.91, and 0.87, respectively. Oxidized BVOC have a nighttime peak in the diurnal profile and drop to nearly
398 zero by noon, likely due to enhanced dilution and quicker oxidation to oxidation states not detectable by PTR-
399 MS.

400 The third factor was identified as BVOC due to the predominance of $C_{10}H_{17}^+$ monoterpene (m/z 137.133) and its
401 fragmentation $C_6H_9^+$ (m/z 81.07) ions in this VOC factor, with correlations of 0.98 and 0.86, respectively.
402 Sesquiterpenes also show a strong correlation with this factor (R=0.80). The average diurnal behavior of BVOC
403 shows an early morning peak, because BVOC, especially monoterpenes, are often stored in vegetation and
404 released at the start of the morning due to sunlight and slight temperature increases (Malik et al., 2023), combined
405 with a shallow boundary layer that keeps emissions near the surface.

406 The fourth factor showed a good correlation with butyric acid $C_3H_5O_3^+$ (m/z 89.024) and $C_4H_5O_3^+$ (m/z 101.024),
407 with R values of 0.75 and 0.72, respectively. The time series of O₃ and this factor showed a good correlation
408 during certain periods. The diurnal cycle of it exhibits a daytime peak, indicating involvement in photochemical
409 oxidation processes. We classified it as aged VOC.

410 The fifth factor, biomass burning VOC, is dominated by propylene glycol $C_3H_9O_2^+$ (m/z 77.06) and orthoacetic
411 acid $C_2H_7O_3^+$ (m/z 79.039), with strong correlations of 0.85 and 0.83, respectively. Additionally, a ring fragment
412 of oxidized syringol, $C_4H_7O_4^+$ (m/z 119.034), and ring fragments of oxidized guaiacol and syringol molecules
413 $C_5H_3O_2^+$ (m/z 95.013), $C_5H_7O_4^+$ (m/z 131.034) and $C_4H_7O_3^+$ (m/z 103.04) contribute smaller fractions but display
414 even higher correlations, with values of 0.90, 0.91, 0.92 and 0.86 (Yee et al., 2013). Compared with the other 4
415 factors, the biomass burning VOC mass spectrum has more oxidized compounds.

416 In late winter and early spring, the first factor was identified as traffic VOC using the same method as in summer,
417 showing high contributions and strong correlations with aromatic hydrocarbon ions, including toluene $C_7H_9^+$ (m/z
418 93.07), C₉ aromatics $C_9H_{13}^+$ (m/z 121.102), and cymene $C_{10}H_{13}^+$ (m/z 133.102) in Figures S7, S8 and Table S5.

419 The second factor, classified as terpenes VOC, was marked by the predominance of monoterpene $C_{10}H_{17}^+$ (m/z
420 137.133) and its fragment $C_6H_9^+$ (m/z 81.07) ions with correlations of 0.90 and 0.89, respectively. Sesquiterpenes
421 also show a strong correlation (R=0.92). The diurnal variation shows both morning and evening peaks, with the
422 morning peak being higher than the evening peak. This pattern differs from typical traffic trends. This pattern is
423 similar to that of limonene from shower gels (Yeoman et al., 2020), which shows higher concentrations in the

424 morning compared to the evening. It correlates with the traffic factor because people typically shower in the
425 morning before leaving home, leading to higher detection. By the evening, the limonene has dissipated.

426 The biomass burning VOC factor included a lot of smaller oxygenated VOC (OVOC) such as 1,3-propanediol
427 $C_3H_9O_2^+$ (m/z 77.06), acetic anhydride $C_4H_7O_3^+$ (m/z 103.04), 2-furoic acid $C_5H_5O_3^+$ (m/z 113.024), maleic acid
428 $C_4H_5O_4^+$ (m/z 117.019), butanedioic acid $C_4H_7O_4^+$ (m/z 119.034), benzoic acid $C_7H_7O_2^+$ (m/z 123.045) (Lemieux
429 et al., 2004) and salicylic acid $C_7H_7O_3^+$ (m/z 139.04). They all show strong correlations ($R=0.85-0.90$) with this
430 factor. Notably, $C_5H_5O_3^+$ and $C_7H_7O_3^+$ are recognized as tracers of biomass burning VOC (Li et al., 2020b;
431 Romanias et al., 2024). It displays a peak during the daytime, possibly due to biomass burning activities in certain
432 areas (e.g., cooking or outdoor grilling), which increase VOC emissions and lead to a daytime peak in the VOC
433 diurnal profile.

434 The fourth factor was dominated by xylene, represented by C_8 -aromatic hydrocarbon $C_8H_{11}^+$ (m/z 107.086), with
435 a correlation of 0.96. This factor also shows a strong correlation with 3-ethyl-pyridine $C_7H_{10}N_1^+$ (m/z 108.081)
436 and the C_9 -aromatic hydrocarbon VOC $C_9H_{13}^+$ (m/z 121.102), with correlations of 0.98 and 0.91, respectively.
437 Xylene and trimethylbenzene are components of flue gases from fossil fuel combustion VOC (Niu et al., 2021).
438 It also displays morning and evening peaks in its diurnal cycle, leading to its identification as a traffic2 VOC.

439 The fifth factor has minimal correlation with most masses, only showing a correlation of 0.73 with benzene ($C_6H_7^+$)
440 and weak correlations with various oxygenated compounds. Therefore, this factor may originate from different
441 low-concentration emission sources. Its diurnal variation shows a small evening peak, likely influenced by traffic
442 or industrial emissions. This factor accounts for $54\% \pm 9\%$ in late winter, decreasing to $23\% \pm 16\%$ in early spring
443 due to the increased temperature (Figure 5), and as background VOC are commonly found to have a high
444 proportion, we classify it as background VOC.

445 The source contributions of VOC vary significantly across seasons, reflecting shifts in emission patterns and
446 atmospheric conditions. In summer, the largest contributor is aged VOC at $42 \pm 18\%$, indicating the dominance
447 of secondary pollutants formed through atmospheric photochemical oxidation processing. Traffic emissions
448 account for $22 \pm 14\%$, while oxidized biogenic VOC make up $13 \pm 13\%$, and fresh BVOC contribute $7 \pm 7\%$.
449 Biomass burning plays a notable role at $16 \pm 15\%$, likely due to outdoor barbeque in warmer months. Winter
450 exhibits a different profile, with background sources dominating at $54 \pm 9\%$, suggesting stable atmospheric
451 conditions. Traffic-related emissions split into two categories—traffic1 ($26 \pm 6\%$) and traffic2 ($7 \pm 6\%$)—possibly
452 reflecting different vehicle types or fuel usage patterns. Monoterpenes VOC remain low ($4 \pm 4\%$), consistent with
453 reduced biogenic activity and from anthropogenic source like personal care products (Wu et al., 2024), while
454 biomass burning contributes $8 \pm 6\%$, potentially from residential heating. In spring, the contributions are traffic1
455 $22 \pm 7\%$, monoterpene VOC increased to $9 \pm 9\%$ as vegetation becomes more active, biomass burning VOC $33 \pm$
456 14% , traffic2 $13 \pm 8\%$, and background $23 \pm 16\%$ (Figure 5).

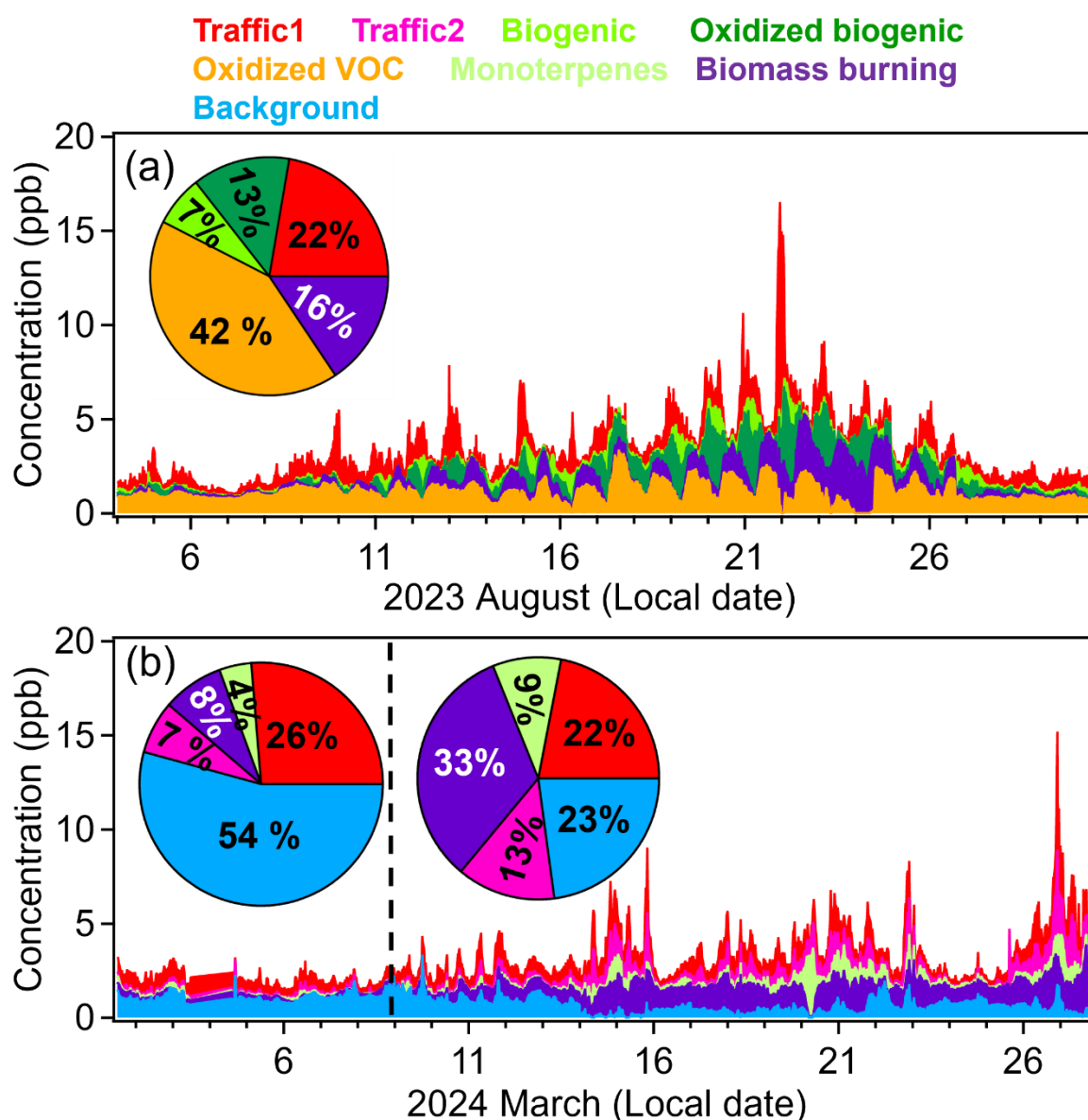


Figure 5: The time series and relative mass contribution (pie charts) of each VOC factor to total VOC concentrations in summer (a), winter (left of the dash line) and spring (right of the dash line) (b).

457 3.2.2 Sources of semi-volatile organic aerosol (SVOA)

458 We included 153 SVOA ions (Table S6) for PMF analysis for summer and 171 ~~VOC-SVOA~~ ions (Table S7) for
 459 winter/spring, excluding abundant ions that could skew results and very low ion signals with minimal impact
 460 (Song et al., 2024). The average semi-volatile organic aerosol concentration was $0.3 \pm 0.2 \mu\text{g m}^{-3}$ in summer, 0.14
 461 $\pm 0.08 \mu\text{g m}^{-3}$ in winter and $0.07 \pm 0.07 \mu\text{g m}^{-3}$ in spring. Through a comprehensive analysis of factor profiles,
 462 diurnal variations, and tracer correlations in summer (Figure S9S11, S10S12, and Table S8) and in winter (Figure
 463 S11S13, S12S14, and Table S9). Five semi-volatile organic aerosol (SVOA) factors were identified as the best
 464 interpretable solution for different seasons.

465 In summer, the first factor showed distinct signals from primary oxidation products of terpenes, including oxidized
 466 monoterpenes $\text{C}_{10}\text{H}_{15}\text{O}_1^+$ ($R=0.93$) and $\text{C}_{10}\text{H}_{17}\text{O}_1^+$ ($R=0.89$) (Li et al., 2020a). While the expected monoterpene
 467 oxidation products are typically $\text{C}_9\text{H}_{15}\text{O}_{1.5}^+$, we found that $\text{C}_9\text{H}_{13}\text{O}_1^+$ and $\text{C}_9\text{H}_{13}\text{O}_2^+$ also correlated well with this

468 factor, with correlation coefficients $R=0.91$ and $R=0.85$, respectively. This suggests that the $C_9H_{15}O_{1-2}^+$
469 compounds may lose hydrogen, forming $C_9H_{13}O_1^+$ and $C_9H_{13}O_2^+$ (Gkatzelis et al., 2018b). Additionally, nitrogen-
470 containing species like $C_9H_{13}N_1O_1$, $C_9H_{12}N_1O_2$, and $C_9H_{13}N_1O_5$ displayed high intensity and significant
471 correlation with this factor, which may indicate they are fragments of monoterpene-derived organic nitrates, such
472 as $C_9H_{15}N_1O_{5.7}$ (Massoli et al., 2018). The diurnal cycle shows a nighttime peak (Figure S10c), which we have
473 attributed this factor to weakly oxidized biogenic organic aerosol (Weakly OBOA) based on the presence of a
474 monoterpene oxidation tracer and the observed diurnal pattern.

475 The second factor includes clear markers of isoprene oxidation products, specifically $C_5H_8O_n$ species (Li et al.,
476 2020a), with $C_5H_9O_6^+$ ($R=0.83$) and $C_5H_9O_3^+$ ($R=0.82$) showing strong correlations (Riva et al., 2016).
477 Additionally, the ion with the highest fraction, $C_3H_5O_4^+$ ($R=0.85$), likely originates from the oxidation of
478 ISOPOOH (Rios, 2018). However, benzoic acid $C_7H_7O_2^+$ ($R=0.95$), showing a strong signal, and phthalic
479 anhydride $C_8H_5O_3^+$ ($R=0.83$) are both known emissions from biomass burning aerosols (Brunns et al., 2017; Koss
480 et al., 2018). $C_6H_8O_5$ ($R=0.84$) (Molteni et al., 2018) is an oxidation product of benzene, while $C_7H_{10}O_6$ ($R=0.84$)
481 as reported by Nakao et al. (Nakao et al., 2011), is an oxidation product of o-cresol, an emission from oxygenated
482 aromatic BBOA. Therefore, we define this factor as mixed oxidized isoprene OA and BBOA.

483 The third factor was identified as BBOA due to its strong correlation ($R=0.88$) with vanillic acid $C_8H_8O_4$ (Fleming
484 et al., 2020) and its prominent fragment ($C_8H_6O_4$) with even higher correlation ($R=0.96$), which constitutes a
485 significant portion of this factor. Additionally, another BBOA tracer, syringic acid ($C_9H_{10}O_5$) (Wan et al., 2019),
486 and its fragment ($C_9H_6O_3$, $R=0.95$), likely formed by the loss of two H_2O molecules, or as a direct BBOA emission
487 (Fleming et al., 2020), further support this identification. Other ions, such as $C_6H_6O_5$ and $C_7H_8O_5$, are oxidation
488 products of guaiacol (Yee et al., 2013). The diurnal cycle of this factor, peaking during the daytime, suggests that
489 barbecue events may be contributing sources during the summer.

490 The fourth factor shows no correlation with other compounds and exhibits a distinct nighttime peak (Figure S10c).
491 However, it correlates strongly with nitrate detected by AMS ($R = 0.71$). This suggests that the factor represents
492 regional background, with its nighttime increase likely influenced by local accumulation effects.

493 The fifth factor was identified as more oxidized monoterpene OA, comprising highly oxidized monoterpene
494 products such as $C_{10}H_{15}O_{3.5}^+$ ($R=0.86, 0.85, 0.84$), diacetin $C_7H_{13}O_5^+$ ($R=0.79$), oxidized molecules of
495 monoterpenes $C_8H_{13}O_2^+$ ($R=0.81$), $C_8H_{13}O_4^+$ ($R=0.80$), and its fragment ($C_8H_{11}O_3^+$, $R=0.83$). Compounds like
496 $C_9H_{13}O_{3.4}^+$ ($R=0.81, 0.78$) likely arise from fragments of the $C_9H_{14}O_n$ series, representing more oxidized
497 monoterpene products that have lost hydrogen. Compared to the diurnal pattern of less oxidized terpene products,
498 this factor's peak displays a delay, suggesting that primary oxidation products form initially and then undergo
499 further oxidation, resulting in more oxidized BOA (More OBOA).

500 In winter and spring, the first factor is identified as night-time aged BBOA due to the presence of distinct BBOA
501 tracers, $C_6H_6N_1O_4^+$ and $C_7H_8N_1O_4^+$ (Figure S12a-S14a), which do not appear in the mass spectra of other factors.
502 Nitrocatechols ($C_6H_5N_1O_4$) originates from anthropogenic activities, including biomass burning and vehicle
503 emissions. Meanwhile, methyl-nitrocatechols ($C_7H_7N_1O_4$) are specific markers for BBOA, as they are formed
504 from m-cresol released during biomass combustion and diesel exhaust (Kourtchev et al., 2016). These tracers also
505 exhibit the same strong correlation of 0.97 with this factor (Table S8). Syringic acid ($C_9H_{10}O_5$) also correlates
506 well ($R=0.70$) with this factor. In terms of its daily cycle did not show peaks during morning or evening rush
507 hours; instead, a peak was observed around 8 p.m., suggesting it aligns more with BBOA. This factor showed a

508 strong correlation with highly oxidized nitrogen-containing compounds and secondary organic aerosols (syringic
509 acid). This factor is more related to highly oxidized nitrogen-containing secondary organic aerosols, indicating
510 that nitrogen-containing compounds produced by BBOA may have undergone significant oxidation by NO₃
511 radicals. Therefore, I identified it as night-time aged BBOA.

512 The second factor was characterized by a high fraction of oleic acid C₁₈H₃₅O₂⁺ (R=0.90), C₁₆H₃₅O₃⁺
513 (C₁₆H₃₃O₂(H₂O)⁺) (R=0.88), C₁₆H₃₃O₂⁺ corresponding to palmitic acid (R=0.54), and C₁₆H₃₁O₁⁺ is the fragment
514 of C₁₆H₃₃O₂⁺ (R=0.54). C₁₈H₃₄O₂ is identified as the cooking tracer oleic acid, while C₁₆H₃₃O₂⁺ serves as another
515 cooking aerosol tracer, corresponding to palmitic acid (Reyes-Villegas et al., 2018; Wang et al., 2020b; Huang et
516 al., 2021). C₁₆H₃₁O₁⁺ is thought to originate from C₁₆H₃₃O₂⁺ due to fragmentation involving the loss of one H₂O
517 molecule. These findings strongly suggest that this factor represents cooking aerosol.

518 The third factor was identified as aged combustion. In this factor, the aromatic hydrocarbon C₇H₉⁺ accounts for a
519 relatively higher fraction and exhibits a strong correlation (R = 0.79). Although C₈H₁₃⁺ does not contribute
520 significantly as C₇H₉⁺, it also shows the same strong correlation. These compounds are attributed to combustion
521 sources (Wang et al., 2022). The ion C₇H₁₀N₁⁺, potentially a fragment of acridine (C₇H₁₂N₁⁺) originating from
522 coal combustion (Wang et al., 2021), exhibits a distinct signal and the highest correlation (R = 0.94). Similarly,
523 C₆H₁₅O₃⁺ (R = 0.93) corresponds to 2-methoxyethyl ether (MXEE), a product of fuel combustion. Monoterpene
524 oxidation products, such as C₁₀H₁₇O₁⁺ (R = 0.86) and C₉H₁₃O₁⁺ (R=0.82), are also observed. This is likely because
525 monoterpenes, serving as biofuel components in engines and boilers, form oxidized monoterpene products when
526 combusted and oxidized (Philippe Dagaut et al., 2024). Additionally, benzocaine C₉H₁₂N₁O₂⁺ exhibits strong
527 correlation (R = 0.80) with this factor and is likely a product of oxidized combustion processes.

528 The fourth factor has C₆ carboxylic acids (C₆H₇O₅⁺) which is the phenol oxidation products with OH radicals in
529 the low-NO_x system, and C₇H₉O₅⁺ denoted as the guaiacol with OH adduct. Propanedioic acid (C₃H₅O₄⁺),
530 pentanedione (C₄H₅O₃⁺), and 2-oxopentanedioic acid C₅H₇O₄⁺ are fragments derived from the OH oxidation
531 products of biomass burning VOC (BBVOC) such as guaiacol and syringol (Yee et al., 2013). Additionally,
532 C₆H₆O₂ is an OH radical oxidation product from phenol. A higher fraction of 2,5-di-(hydroxymethyl)furan
533 C₆H₉O₃⁺ was observed, which may result from C₆H₇O₂⁺ binding with a water molecule. These photochemical
534 products, formed from BBVOC oxidation by OH radicals, confirm that this factor represents aged BBOA. All the
535 aforementioned ions exhibit a strong correlation of approximately 0.85 with this factor, as shown in Table S2.
536 Furthermore, its diurnal pattern, with a peak at 15:00 during the day, leads to its identification as day-time aged
537 BBOA.

538 The fifth factor shows a very strong correlation with stearic acid C₁₈H₃₇O₂⁺ (R = 0.95), C₁₆H₃₃O₂(H₂O)⁺ (R = 0.91),
539 C₁₈H₁₅O₁⁺ (R = 0.90), C₁₉H₁₅O₁⁺ (R = 0.88), and oleic acid C₁₈H₃₅O₂⁺ (R = 0.88). However, these compounds do
540 not account for significant fractions in this factor's mass spectrum as they do in factor 2's mass spectrum. Notably,
541 trimethoxy methane C₄H₁₁O₃⁺ is a key ion in this factor but contributes minimally to others and shows no
542 correlation with the factor (R = 0.02). While the composition includes unrelated compounds, its strong correlation
543 with sulfate detected by AMS (R=0.74) suggests a regional background origin, with the nighttime peak indicating
544 local accumulation effects.

545 During summer, the composition of SVOA includes 11 ± 15% weakly OBOA, 16 ± 15% oxidized isoprene &
546 BBOA (mixture of oxidized isoprene OA and BBOA), 25 ± 21% BBOA, 30 ± 22% attributed to regional
547 background sources, and 18 ± 16% to More OBOA (Figure 6). Although cooking-related SVOA ions were present

548 during summer, the higher contribution of biogenic oxidation products in overlapping mass spectral regions likely
 549 reduced the statistical separability of a distinct cooking factor in the SVOC PMF analysis (Zhu et al., 2018;
 550 Coggon et al., 2024a). In winter, nighttime aged BBOA accounts for $10 \pm 9\%$, cooking OA contributes $4 \pm 5\%$,
 551 aged combustion OA makes up $9 \pm 10\%$, daytime aged BBOA constitutes the largest fraction at $55 \pm 21\%$, and
 552 regional background sources contribute $23 \pm 17\%$. In spring, nighttime aged BBOA accounts for $12 \pm 12\%$,
 553 cooking OA contributes $11 \pm 12\%$, aged combustion OA makes up $24 \pm 18\%$, daytime aged BBOA constitutes
 554 the largest fraction at $46 \pm 25\%$, and regional background sources contribute $7 \pm 9\%$.

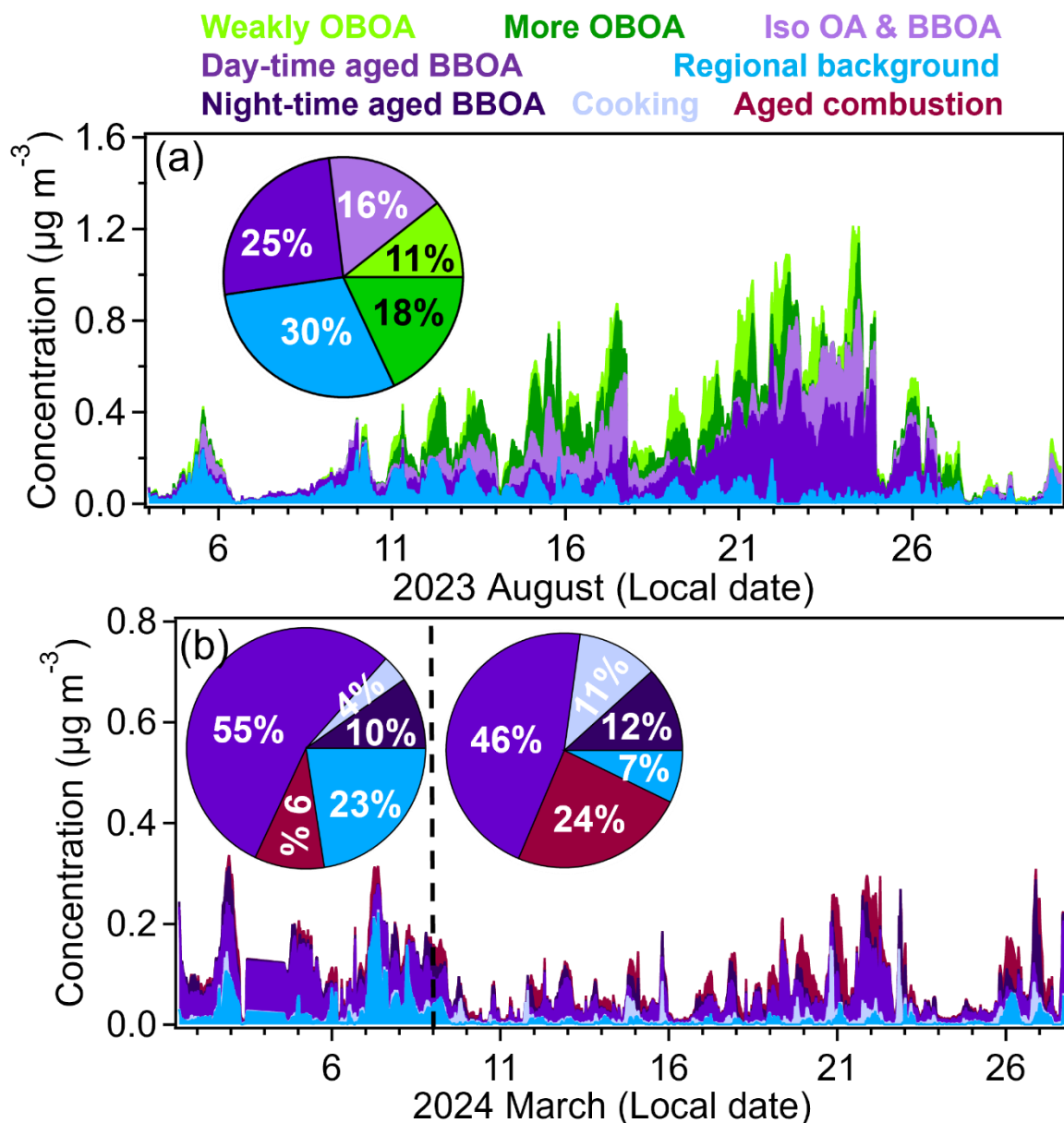


Figure 6: The time series and relative mass contributions (pie charts) of each SVOA factor to total SVOA concentrations in summer (a), winter (left of the dash line), and spring (right of the dash line) (b).

555 3.2.3 Sources of organic aerosol particles

556 This study thoroughly examined source factor profiles, diurnal patterns, and correlations with tracers
 557 (FigureS13FigureS15-16, S14S17-18, S15and S19-20, S16 and S17) for OA particles. The average organic
 558 aerosol concentration was $4.3 \pm 2.9 \mu\text{g m}^{-3}$ in summer, $3.4 \pm 1.7 \mu\text{g m}^{-3}$ in winter and $1.8 \pm 1.8 \mu\text{g m}^{-3}$ in spring.

559 Five OA factors were identified as the optimal interpretable solutions for summer and winter/spring, respectively.
560 [Alternative PMF solutions with different factor numbers were systematically evaluated based on Q/Q_{exp} behavior,](#)
561 [factor interpretability, and tracer correlations: details are provided in the Supplement \(Figure S14\).](#)

562 In summer, the first factor was identified as cooking organic aerosol (COA), based on its high H: C ratio (1.82),
563 low O: C ratio (0.19) (Figure [S14a](#)[S17a](#)), higher contributions at m/z 55 (C₃H₃O⁺) and m/z 57 (C₃H₅O⁺), and the
564 mass spectrum dominated by hydrocarbon ions. These characteristics are consistent with reported COA in urban
565 areas (Elser et al., 2016; Äijälä et al., 2017; Liu et al., 2018). Additionally, fatty acid (C₁₆H₃₅O₃⁺) detected by
566 CHARON-PTR showed a moderate correlation (R = 0.54) with the COA time series (Figure [44b](#)[17b](#)). The second
567 factor is characterized by a mass spectrum also dominated by hydrocarbon ions, a similar O: C ratio, and a high
568 O: C ratio, but with higher contributions at m/z 55 (C₄H₇⁺) and m/z 57 (C₄H₉⁺) (Elser et al., 2016). These features
569 are consistent with the characteristics of hydrocarbon-like organic aerosol (HOA) which is related to traffic.
570 additionally, HOA shows a good correlation (R= 0.66) with the eBC time series. The third factor is assigned to
571 Biogenic secondary organic aerosol (BOA), based on its H: C ratio of 1.63 and O: C of 0.44. The O/C ratio falls
572 within the range typically associated with semi-volatile oxidized organic aerosol (SVOOA), which is
573 approximately 0.35 ± 0.14 (Setyan et al., 2012). And it has a good correlation of 0.86 with monoterpene oxidation
574 products (pinonaldehyde) in CHARON-PTR. BOA's diurnal pattern (Figure [S14e](#)[S17c](#)) shows an increase starting
575 at 8 pm, reaching its peak at 7 am. This trend aligns with the nighttime oxidation process of monoterpenes,
576 supporting its identification as BOA. The fourth factor was identified as aged biomass burning organic aerosol
577 (BBOA) because its O/C ratio of 0.597 is slightly higher than that of fresh BBOA (0.15-0.5) and falls within the
578 range of aged BBOA (0.5-0.87) (Ortega et al., 2013). Its diurnal shows a small peak at 3 pm and a higher peak at
579 10 pm, the nighttime peak indicates that fresh BBOA happened rapid dark aging process (Kodros et al., 2020).
580 And it shows a strong correlation (R=0.93) with BBOA tracer levoglucosan detected by CHARON-PTR. therefore,
581 the fourth factor is identified as aged BBOA. The fifth factor has the lowest H: C ratio (1.43) and the highest O:C
582 ratio 0.75, which falls within the range of low-volatility oxygenated organic aerosol (LVOOA) (0.6-1.0) (J. L.
583 Jimenez et al., 2009). LVOOA is dominated by CO⁺ and CO₂⁺ and shows a strong correlation (R=0.70) with O₃,
584 indicating that it is associated with photochemical oxidation processes (Kumar et al., 2016). Its diurnal pattern
585 shows a daytime peak. These characteristics align well with the typical properties of LVOOA, leading to its
586 identification as LVOOA. To ensure that every tracer detected by CHARON-PTR and correlated with AMS-PMF
587 factors is representative, we compared different related fatty acids, toluene and trimethyl benzene, different
588 monoterpene oxidation products, and different BBOA tracers. All of them showed good time-series correlations
589 (Figure [S16](#)[S19](#)).

590 In winter, we identified all the factors using the same method as in summer. The difference is that the traffic
591 diurnal cycle (Figure [S15e](#)[S18c](#)) exhibits distinct peaks during the morning and evening rush hours. Fresh BBOA
592 shows an evening peak, indicating evening residual heating activities. Aged BBOA is characterized by its
593 correlation with C₆H₇O₅⁺, which we identified as an oxidation product of BBOA in the CHARON-PTR section.
594 its diurnal pattern is very flat, suggesting it may be associated with regional background levels or long-range
595 transport. for LVOOA, NH₄⁺ is used as an indicator, as it correlates strongly with inorganic aerosol during autumn
596 and winter (Freney et al., 2011). Other different OA factors time series shown in Figure [S17](#)[S20](#).

597 In summer, OA contributions are as follows: traffic 8 ± 8%, cooking 11 ± 13%, BOA 22 ± 14%, aged BBOA 25
598 ± 21%, and LVOOA 33 ± 20%. In winter, the contributions are: traffic 5 ± 4%, cooking 12 ± 12%, fresh BBOA

599 $13 \pm 9\%$, aged BBOA $36 \pm 12\%$, and LVOOA $33 \pm 17\%$. In spring, the contributions are: traffic $9 \pm 7\%$, cooking
 600 $19 \pm 16\%$, fresh BBOA $27 \pm 17\%$, aged BBOA $37 \pm 19\%$, and LVOOA $9 \pm 10\%$ (Figure 7).

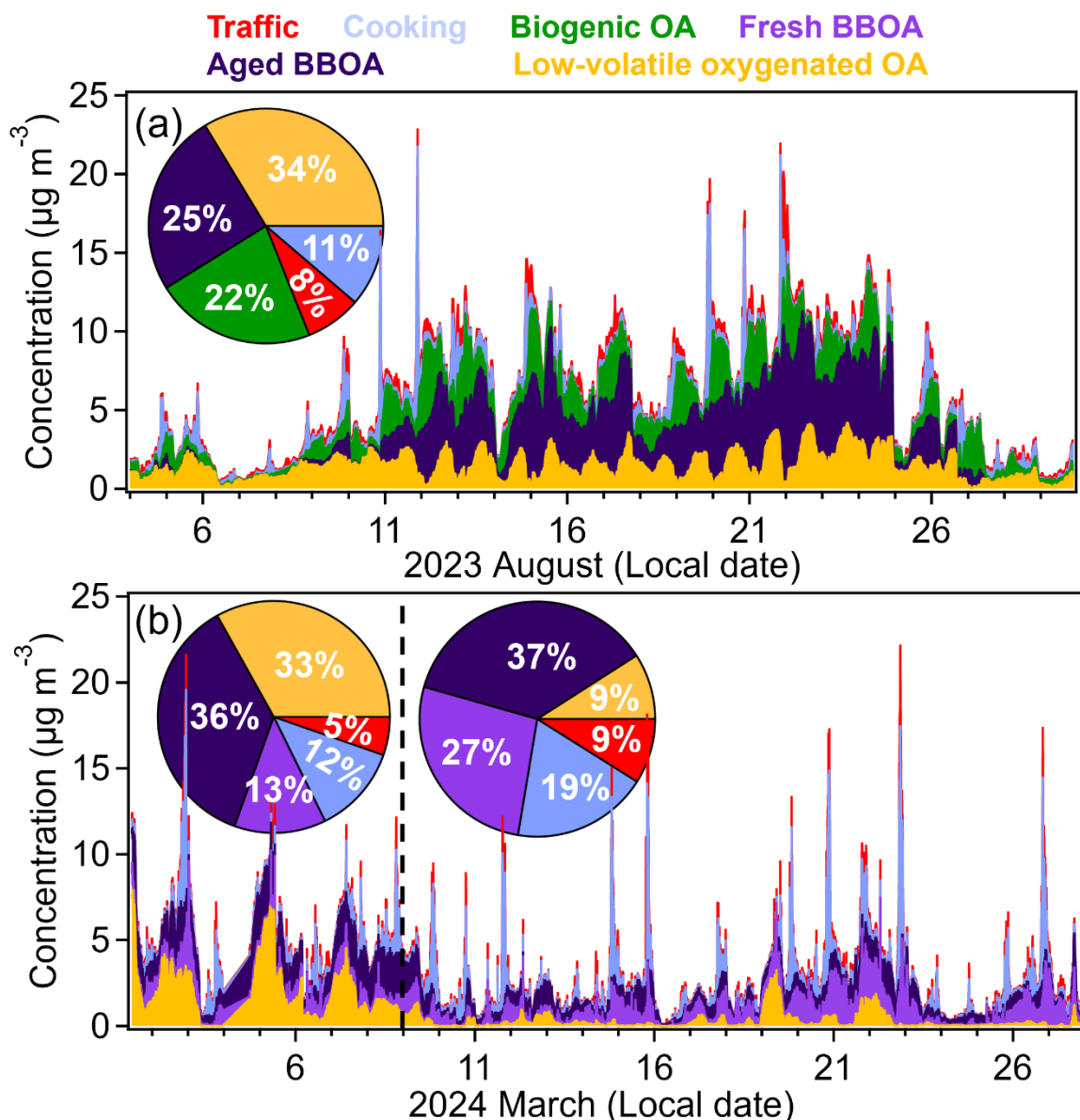


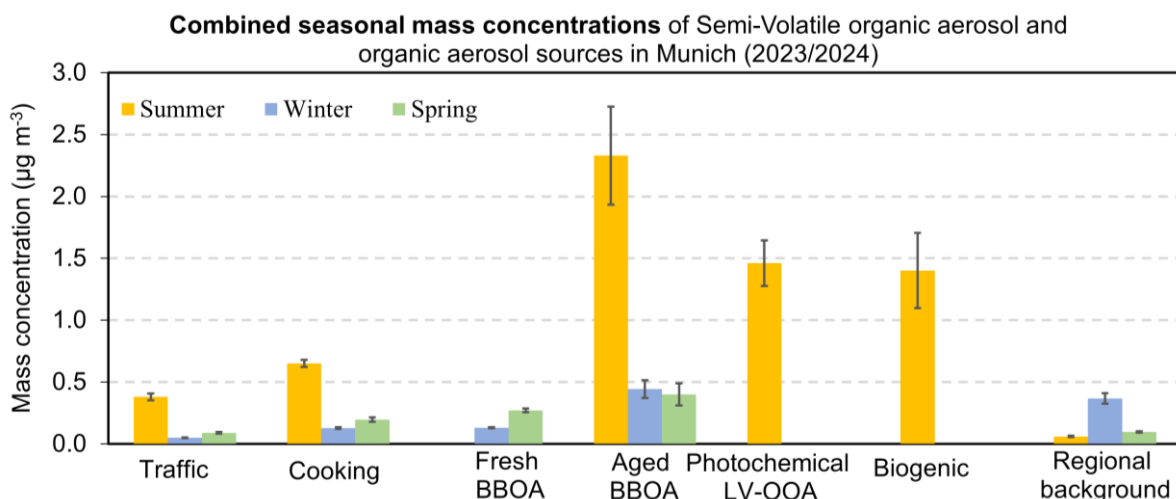
Figure 7: The time series and relative mass contributions (pie charts) of each OA factor to total OA concentrations in summer (a), winter (left of the dash line), and spring (right of the dash line) (b).

601
 602 Previous PMF studies in Stuttgart and Karlsruhe identified consistent summer source patterns: traffic-related OA
 603 contributes less than 10%, SV-OOA accounts for approximately 16%, while LV-OOA dominates at around 75%
 604 of OA mass. This LV-OOA prevalence indicates strong biogenic influence from regional vegetation and
 605 photochemical processes enhanced by higher summer temperatures. In Stuttgart, elevated winter $PM_{2.5}$ stems
 606 primarily from biomass burning and residential heating, evidenced by enhanced levoglucosan and nitrated phenol
 607 signals, alongside increased traffic-related primary OA (POA). Both traffic OA and BBOA contribute
 608 substantially, though LV-OOA remains significant. Karlsruhe experiences similar source patterns with increased
 609 residential heating, traffic emissions, and coal combustion from industrial sources, but benefits from less severe
 610 inversion and stagnation conditions, resulting in lower overall concentrations. Munich's intermediate winter

611 pollution levels suggest a source composition transitioning between these profiles, warranting detailed PMF
 612 analysis to characterize its specific emission contributions and compare with the established patterns in Stuttgart
 613 and Karlsruhe.

614 PMF source apportionment reveals strong seasonal dependencies in organic aerosol composition, with summer
 615 conditions driving the majority of aerosol burden in Munich. Summer demonstrates the highest concentrations
 616 across all source categories, dominated by aged BBOA ($2.3 \mu\text{g m}^{-3}$) as the largest single contributor due to
 617 barbecue charcoal combustion. Photochemical LV-OOA ($1.5 \mu\text{g m}^{-3}$) and biogenic emissions ($1.4 \mu\text{g m}^{-3}$) emerge
 618 exclusively during summer, reflecting enhanced secondary aerosol formation under high temperatures and intense
 619 solar radiation that promote both biogenic emissions and photochemical processing. In contrast, late winter and
 620 spring show dramatically reduced organic aerosol levels, with late winter contributions limited primarily to
 621 regional background ($0.4 \mu\text{g m}^{-3}$) and minimal aged BBOA ($0.4 \mu\text{g m}^{-3}$). Traffic and cooking emissions remain
 622 consistently minor throughout all seasons ($\leq 0.7 \mu\text{g m}^{-3}$), suggesting these local primary sources are less
 623 significant compared to secondary formation processes and regional biomass burning influences.

624 SVOA and OA composition exhibits distinct seasonal patterns driven by varying source emissions and
 625 atmospheric processing. Summer periods show elevated OA concentrations due to enhanced photochemical
 626 oxidation under high solar radiation, promoting secondary organic aerosol formation (Figure 8). Biogenic sources
 627 contribute significantly during summer through increased vegetation emissions. Rapid atmospheric oxidation
 628 transforms fresh BBOA to aged BBOA, explaining the predominance of aged BBOA despite active barbecue
 629 activities. In late winter, residential heating dominated fresh BBOA emissions. During early spring, both heating
 630 and barbecue emissions contributed to fresh BBOA, with the latter increasing as temperatures rose. Consequently,
 631 Fresh BBOA concentrations increased from late winter to early spring. However, Fresh BBOA became less
 632 detectable in peak summer due to accelerated aging processes under higher temperatures and enhanced
 633 photochemical activity. Late winter and spring show substantial aged BBOA from residential heating activities.
 634 Cooking and traffic emissions remain consistent year-round sources, though their oxidation efficiency increases
 635 significantly in summer compared to winter and early spring when photochemical processes are less active.



636
 637 **Figure 8: Comprehensive seasonal mass contributions of SVOA and OA sources in Munich summer, winter and spring**
 638 **time (Source categories combine factors from Charon-PTR-MS and HR-TOF-AMS: Aged BBOA (day-time aged**
 639 **BBOA, night-time aged BBOA, and IsoOA & BBOA from Charon; aged BBOA from AMS), Biogenic OA (weakly**
 640 **OBOA and More OBOA from Charon; BOA from AMS), with remaining sources combined similarly). Please note,**

641 that the total OA concentrations were $4.3 \pm 2.9 \mu\text{g m}^{-3}$ in summer, $3.4 \pm 1.7 \mu\text{g m}^{-3}$ in winter, and $1.8 \pm 1.8 \mu\text{g m}^{-3}$ in
642 spring.

643 3.3 Seasonal strong biomass burning aerosol events

644 PMF analysis of AMS mass spectra reveals that aged BBOA substantially contributes to total OA with seasonal
645 variations: $25 \pm 21\%$ in summer, $36 \pm 12\%$ in winter, and $37 \pm 19\%$ in spring. Two prominent BBOA events were
646 observed during August 22nd-24th (OA: $7.9 \pm 1.7 \mu\text{g m}^{-3}$) and March 7th-9th (OA: $3.3 \pm 1.3 \mu\text{g m}^{-3}$).

647 During August 2023, aged BBOA showed strong correlations with multiple biomass burning indicators (Figure 9
648 and Table S10). The high correlation with eBC ($R=0.75$) suggests significant light-absorbing carbon from
649 combustion processes. Primary biomass burning tracers showed excellent correlations: levoglucosan ($\text{C}_6\text{H}_{11}\text{O}_5^+$,
650 $R=0.93$) and syringic acid ($\text{C}_9\text{H}_{11}\text{O}_5^+$, $R=0.84$), confirming fresh biomass burning emissions. The strong
651 correlation with atmospheric oxidation products such as $\text{C}_6\text{H}_7\text{O}_5^+$ ($R=0.88$, phenol oxidation products from OH
652 radical reactions under low- NO_x conditions) and $\text{C}_7\text{H}_9\text{O}_5^+$ ($R=0.87$, guaiacol-OH oxidation products) indicates
653 significant photochemical aging processes during summer. Notably, aged BBOA correlated strongly with
654 barbecue charcoal combustion tracers including formaldehyde ($R=0.80$) (Kabir et al., 2010), coniferyl alcohol
655 ($\text{C}_{10}\text{H}_{13}\text{O}_3^+$, $R=0.90$), pinic acid ($\text{C}_9\text{H}_{15}\text{O}_4^+$, $R=0.76$), and homovanilic acid ($\text{C}_9\text{H}_{11}\text{O}_4^+$, $R = 0.83$) (Vicente et al.,
656 2018). Several of these tracers are considered more specific to charcoal combustion than to traffic or fossil-fuel
657 sources, and the pronounced evening maximum of the factor is consistent with typical barbecue activity patterns,
658 supporting a local grilling-related origin. These consistently high correlations ($R > 0.75$) strongly suggest that the
659 aged BBOA factor during summer months is predominantly attributed to barbecue activities, as these compounds
660 are characteristic markers of charcoal and wood combustion used in outdoor cooking rather than other biomass
661 burning sources. Backward trajectory analysis combined with VIIRS fire radiative power (FRP) data for August
662 suggests negligible influence from regional wildfires along the air-mass transport pathways (Fig. S21a). Although
663 several fire detections classified as “unknown” sources were observed (Fig. S21b), their FRP values were very
664 low, indicating weak fire intensity and suggesting that they are unlikely to contribute substantially to the elevated
665 BBOA levels observed in Munich. However, during the intensive BBOA episode (August 22nd-24th), most tracer
666 correlations decreased slightly, and formaldehyde showed no correlation with aged BBOA ($R= -0.20$) in Table
667 S10. This suggests that during high-concentration events, different source contributions alter the chemical
668 fingerprint, possibly indicating the influence of additional fresh emissions or changes in atmospheric processing
669 conditions. Back trajectory analysis during the strong BBOA event shows that 51% of air masses originated from
670 long-range transport near the Belgium border (average BBOA: $5.3 \mu\text{g m}^{-3}$), while 15% from the Bavarian region
671 exhibited the highest concentrations ($7.3 \mu\text{g m}^{-3}$) in Figure S18S22. Given the absence of wildfire sources and the
672 strong correlations with barbecue charcoal combustion tracers, we attribute the elevated concentrations primarily
673 to outdoor barbecue charcoal combustion emissions.

674 In the whole March 2024, aged BBOA exhibited markedly different correlation patterns, indicating distinct
675 sources and processes. The weaker correlation with eBC ($R=0.39$) suggests different combustion characteristics
676 compared to summer. Most importantly, aged BBOA showed poor correlations with barbecue charcoal
677 combustion tracers: formaldehyde ($R=0.14$), coniferyl alcohol ($R=0.47$), pinic acid ($R=0.41$), and homovanilic
678 acid ($R=0.51$). The dramatic decrease in these correlations compared to summer values indicate minimal

679 contribution from outdoor cooking activities during winter months. Primary biomass burning markers also showed
680 reduced correlations: levoglucosan ($R=0.30$), and syringic acid ($C_9H_{11}O_5^+$, $R=0.24$), suggesting different emission
681 sources or processing pathways. Conversely, aged BBOA maintained strong correlations with guaiacol oxidation
682 products: $C_6H_7O_5^+$ ($R=0.80$) and $C_7H_9O_5^+$ ($R=0.74$). This pattern strongly indicates that winter aged BBOA
683 primarily originates from residential heating emissions that have undergone atmospheric oxidation (Kodros et al.,
684 2020). The guaiacol derivatives are characteristic markers of wood combustion for heating purposes, and their
685 predominant correlations with aged BBOA confirm this source attribution. In contrast, fresh BBOA showed strong
686 correlations with barbecue charcoal combustion tracers: coniferyl alcohol ($R=0.69$), pinic acid ($R=0.68$), and
687 homovanilic acid ($R=0.67$), as well as primary biomass burning markers including levoglucosan ($R=0.72$) and
688 syringic acid ($R=0.62$). Notably, fresh BBOA showed weak correlation with the aged oxidation products ($C_6H_7O_5^+$
689 and $C_7H_9O_5^+$) that strongly correlated with aged BBOA. This divergent correlation pattern suggests that fresh
690 BBOA during late winter and early spring is associated with primary biomass-burning emissions, likely dominated
691 by residential heating under weak photochemical conditions, with additional contributions from barbecue charcoal
692 combustion as temperatures increase. Because these sources share similar biomass-burning signatures, a
693 separation between residential heating and barbecue emissions has significant uncertainty. emitted from
694 residential heating or barbecue charcoal combustion during late winter and early spring undergoes The observed
695 separation between fresh and aged BBOA characteristics reflects slower atmospheric aging during colder periods
696 compared to summer conditions, resulting in a clear separation between fresh and aged BBOA characteristics.

697 The intensive episode analysis (March 7th-9th, 2024) revealed correlation patterns consistent with the monthly
698 analysis (Table S10), reinforcing the conclusion that seasonal BBOA sources shift from barbecue charcoal
699 combustions in summer to residential heating in winter. During this episode, aged BBOA maintained strong
700 correlations exclusively with guaiacol oxidation products ($C_6H_7O_5^+$ and $C_7H_9O_5^+$), consistent with the monthly
701 pattern. However, fresh BBOA exhibited notably selective correlations, showing moderate relationships only with
702 coniferyl alcohol ($R=0.65$) and levoglucosan ($R=0.62$), while displaying weak or negligible correlations with
703 other tracers. The limited correlation pattern of fresh BBOA can be attributed to its substantially lower
704 concentration compared to aged BBOA during this period (Table S10). When aged BBOA dominates the total
705 BBOA mass, the temporal variability of most tracers is primarily governed by the aged component, effectively
706 masking the correlation signals from fresh BBOA. As a minor constituent, fresh BBOA's true relationships with
707 various tracers become statistically obscured, making it challenging to establish robust correlations beyond the
708 most characteristic primary emission markers (i.e., levoglucosan and coniferyl alcohol). This phenomenon
709 highlights the importance of aged BBOA as the dominant source during winter heating periods, while fresh
710 emissions represent localized, transient contributions that are rapidly diluted within the regional aged aerosol
711 background. Back trajectory analysis reveals distinctly different transport patterns compared to summer. Winter
712 air masses predominantly followed three clusters: Cluster 1 (32%) transported through Czechia with BBOA
713 concentrations of $2.3 \mu\text{g m}^{-3}$, Cluster 2 (14%) originating from Poland passing through Czechia ($1.8 \mu\text{g m}^{-3}$), and
714 Cluster 3 (19%) from the Belarus-Poland border passing through Czechia and Austria ($1.1 \mu\text{g m}^{-3}$) in Figure
715 S18S22. The dominance of Czechia-influenced trajectories (65%) contrasts sharply with summer patterns,
716 indicating significant contributions from Central European residential heating emissions. The prevalence of aged
717 BBOA in these air masses suggests substantial accumulation of Aged BBOA during long-range transport. Notably,

718 Cluster 2 exhibited elevated fresh BBOA concentrations, evidenced by lower O:C ratios, indicating recent biomass
 719 burning emissions from residential heating activities along the Polish transport pathway.

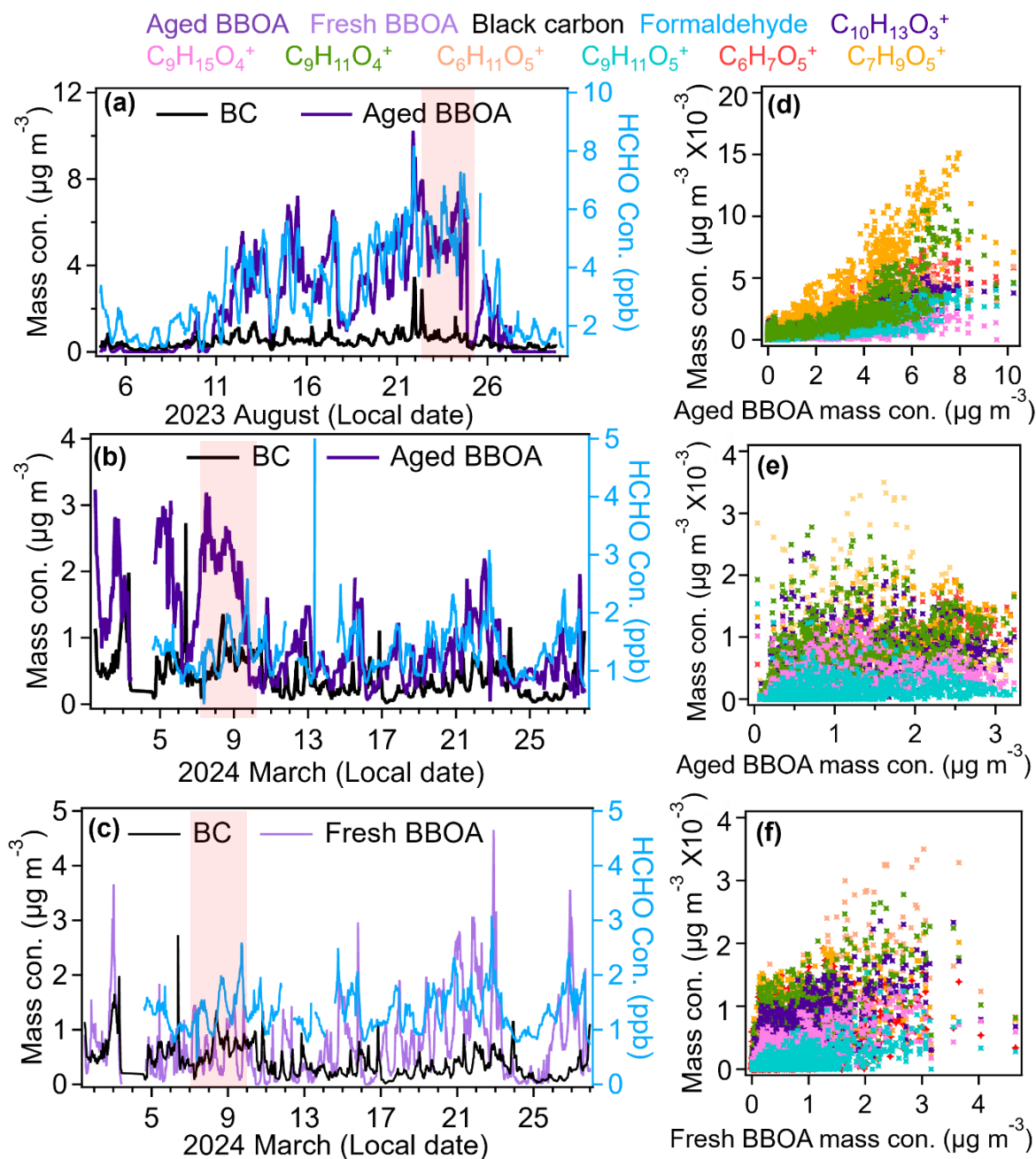


Figure 9. Time series of aged BBOA, black carbon, and formaldehyde during summer (August 2023, a) and winter/spring (March 2024, b) periods and fresh BBOA during March 2024 (c); Scatter plots showing correlations between aged BBOA and barbecue charcoal combustion tracers ($\text{C}_{10}\text{H}_{13}\text{O}_3^+$, $\text{C}_9\text{H}_{15}\text{O}_4^+$, $\text{C}_9\text{H}_{11}\text{O}_4^+$), and biomass burning tracers ($\text{C}_6\text{H}_{11}\text{O}_5^+$, $\text{C}_9\text{H}_{11}\text{O}_5^+$, $\text{C}_9\text{H}_7\text{O}_3^+$, $\text{C}_6\text{H}_7\text{O}_5^+$, $\text{C}_7\text{H}_9\text{O}_5^+$) in summer (d), in winter (e) and Fresh BBOA correlated with all the tracers (f). Strong BBOA events are in red shade.

720 4. Conclusions

721 This study investigates the sources, concentrations, and seasonal variations of VOC, SVOA, and OA in an urban
 722 street canyon of the third largest German city, Munich, using a combination of online mass spectrometric

723 observations and PMF based source apportionment. The results reveal a complex interplay between anthropogenic
724 and biogenic sources, as well as atmospheric photochemical aging that governs the composition and evolution of
725 the atmospheric pollutants in the urban street canyon.

726 The PM_{2.5} analysis reveals Munich's distinctive air quality profile for different seasons. During summer, Munich's
727 PM_{2.5} concentrations ($6.7 \pm 3.7 \mu\text{g m}^{-3}$) are comparable to neighboring German cities like Stuttgart ($7.1 \pm 3.3 \mu\text{g}$
728 m^{-3}) and Karlsruhe ($7.0 \pm 3.5 \mu\text{g m}^{-3}$), also reflecting similar regional background conditions. Winter shows
729 greater divergence: Munich's levels ($13.0 \pm 7.4 \mu\text{g m}^{-3}$) exceed Karlsruhe's ($5.6 \pm 4.9 \mu\text{g m}^{-3}$) but remain
730 substantially lower than Stuttgart's pollution ($27.0 \pm 11.9 \mu\text{g m}^{-3}$) also caused by stronger industrial sources in a
731 basin like topography (Huang et al., 2019). This intermediate profile becomes even more significant when
732 considering Munich's status as Germany's third-largest city, with a dense urban population and strong economic
733 activity generating complex emission patterns, however, with less classical emissions from heavy
734 industry. Compared to other European cities - Paris with winter PM_{2.5} maximum of $15 \mu\text{g m}^{-3}$, Berlin's winter PM_{2.5}
735 episodes above $15 \mu\text{g m}^{-3}$ (the World Health Organization (2021) recommended daily limit), or Bern's winter 14
736 $\mu\text{g m}^{-3}$ average (Bressi et al., 2013; Grange et al., 2021; Renard et al., 2024) - Munich represents a critical test
737 case with high population density, thriving industries and tourism.

738 Our findings identify and quantify a pronounced seasonal regime shift in organic aerosol composition. While a
739 substantial anthropogenic baseline from traffic is persistent, the system transitions from a winter regime
740 dominated by primary biomass burning aerosols (BBOA contributing up to 64% of OA) to a summer regime
741 governed by photochemical aging (LVOOA at 33%) and formation of secondary biogenic aerosol. Critically, we
742 demonstrate that biomass burning is not confined to the heating season. The significant and rising contribution
743 from barbecue emissions in spring and summer reveals an underappreciated, health-sensitive emission source
744 (Lenssen et al., 2022; Xu et al., 2023; Gruber and Kalamas, 2024).

745 The seasonal evolution of BBOA provides critical insights into its atmospheric processing. The presence of both
746 fresh and aged BBOA in winter (fresh: $13 \pm 9\%$; aged: $36 \pm 12\%$) and spring (fresh: $27 \pm 17\%$; aged: $37 \pm 19\%$)
747 contrasts sharply with the aerosol composition in summer, where only aged BBOA ($25 \pm 21\%$) is detected. This
748 pattern strongly indicates that primary biomass burning emissions undergo rapid atmospheric oxidation in summer,
749 with substantial conversion to the aged type driven by enhanced photochemical activity (e.g., higher temperatures,
750 radiation, and O₃ levels). This rapid aging process for BBOA (Kodros et al., 2020; Li et al., 2023) presents a
751 marked contrast to the typically slower, multi-generational oxidation pathway of anthropogenic VOCs from traffic
752 (Srivastava et al., 2022), which require substantial atmospheric processing to form condensable SOA. A key
753 implication of this finding is that if biomass burning OA persists in the atmosphere despite rapid aging processes,
754 then mitigation strategies targeting primary biomass burning emissions could yield more immediate air quality
755 benefits. We identified nocturnal oxidation of biogenic VOC as a significant SOA formation pathway in summer.
756 The substantial contribution of biogenic VOCs (oxidized BVOC: $13 \pm 13\%$, and BVOC: $7 \pm 7\%$), coupled with
757 BOA from oxidized monoterpenes ($22 \pm 14\%$), demonstrates that nocturnal oxidation (primarily by O₃ and NO₃
758 radicals) generates secondary aerosol yields comparable those from daytime photochemical production (e.g.,
759 LVOOA at $33 \pm 20\%$). Consequently, monoterpene emission profiles must be treated as a critical air quality
760 parameter and considered in urban vegetation management (Ren et al., 2014). It should be taken into account that
761 the urban green can have positive but also negative impact on the ~~pollution~~ levels of aerosol particles. Urban green
762 infrastructure provides multiple environmental and health benefits, but may also influence secondary aerosol and

763 [ozone formation depending on species-specific BVOC emission characteristics \(Ahn et al., 2022; Wang et al.,](#)
764 [2025; Ma et al., 2025\)](#). For example, urban forestry programs can preferentially plant lower-monoterpene-emitting
765 [species such as Ginkgo biloba or Taxus cuspidata instead of high-emitting conifers such as Metasequoia](#)
766 [glyptostroboides in NO_x-rich street canyons, or adjust pruning and replacement strategies accordingly, which may](#)
767 [help balance air-quality impacts while preserving ecosystem benefits \(Maison et al., 2024\)](#).

768 Previous studies in Stuttgart and Karlsruhe (Huang et al., 2019; Song et al., 2022; Zhang et al., 2024) identified
769 traffic-related OA contributions consistently at or below 10% during summer. Munich exhibits similar patterns,
770 with traffic OA contributing $8 \pm 8\%$ in summer, $5 \pm 4\%$ in winter, and $9 \pm 7\%$ in spring. This consistency across
771 all three cities in southwest Germany indicates that traffic is a minor OA component, exhibiting only relatively
772 small seasonal variations. The most significant difference emerges in the abundance of LV-OOA. In Stuttgart and
773 Karlsruhe, LV-OOA dominates summer OA with approximately 75%, reflecting strong biogenic influence from
774 regional vegetation and photochemical processes enhanced by higher temperatures. In contrast, Munich's LV-
775 OOA remains substantially lower and relatively stable for different seasons ($33 \pm 20\%$ summer, $33 \pm 17\%$ winter,
776 $9 \pm 10\%$ spring), indicating either reduced biogenic precursor emissions or weaker photochemical oxidation
777 despite comparable regional conditions. In Stuttgart, elevated winter PM_{2.5} stems primarily from biomass burning
778 and residential heating, evidenced by enhanced levoglucosan and nitrated phenol signals. Both traffic OA and
779 BBOA contribute substantially to winter pollution. Karlsruhe exhibits similar patterns, with residential heating,
780 traffic emissions, and coal combustion from industrial sources driving winter PM_{2.5} increases. Munich's source
781 profile diverges markedly from both cities. BBOA contributes substantially more to Munich's OA composition
782 year-round compared to Stuttgart and Karlsruhe. Summer shows notable BBOA contribution (aged BBOA $25 \pm$
783 21% combined with BOA $22 \pm 14\%$), and winter BBOA dominance increases dramatically (fresh BBOA $13 \pm 9\%$
784 plus aged BBOA $36 \pm 12\%$). Spring displays the highest BBOA contribution (fresh BBOA $27 \pm 17\%$ plus aged
785 BBOA $37 \pm 19\%$), indicating sustained biomass burning influence extending beyond residential heating into
786 recreational activities. This persistent, elevated BBOA signature distinguishes Munich as a BBOA-dominated
787 system, contrasting with the LV-OOA-dominated profiles of Stuttgart and Karlsruhe, and suggests that biomass
788 burning requires year-round mitigation strategies in Munich.

789 In summary, this work reveals the dynamic chemical evolution of urban aerosol. The interplay between primary
790 emissions from heating and cooking, the relatively constant traffic baseline, and the seasonally-modulated
791 photochemical and nocturnal monoterpene chemistry creates a complex but decipherable pollution phenotype.
792 Future research should prioritize tracking the atmospheric evolution of key source markers (e.g., from barbecues
793 especially in summer and spring) to constrain their aging timescales and health-relevant properties. Integrating
794 these process-level insights is paramount for refining air quality models like PALM-4U (Zhang et al., 2024; Resler
795 et al., 2024; Samad et al., 2024) to accurately predict effectivity of measures to improve air quality in future urban
796 scenarios.

797 **Conflict of interests statement:**

798 Two co-authors are co-editors of ACP but the authors declare that there is no conflict of interests.

799 **Author contributions**

800 FK, JC, and HS conceived the concept, planned, and organized the campaign. YXL did the AMS and PTR-MS
801 measurements, analyzed most of the data and wrote the manuscript with contributions from all co-authors. HS
802 planned and organized the measurements, took care of the particle number, size and additional trace gas
803 measurements. HZ, SA, AW, JC and FK supported instrument set up and conducted lidar measurements. XS,
804 YWL and FK checked and calibrated the instruments during the measurements. JBS, ZA, and JS contributed to
805 data analysis. TL contributed to planning of the measurement campaign and reviewed the manuscript.

806 **Data availability**

807 The data used in this study is available at the KIT data repository KITopen data (doi will be added here).

808 **Acknowledgement**

809 We gratefully acknowledge the support by the meteorological department of the Ludwig-Maximilians-University
810 of Munich (Group of Prof. Bernhard Mayer) and especially Markus Garhammer. The support by the technical
811 team (Group of Steffen Vogt) of the Institute of Meteorology and Climate Research Atmospheric Aerosol
812 Research of the Karlsruhe Institute of Technology was extremely helpful.

813 **Funding**

814 The China Scholarship Council (CSC) provided PhD scholarships for Yanxia Li and Xuefeng Shi. The KIT
815 Graduate School for Climate and Environment (GRACE) supported Yanxia Li. The KIT funded the campaign in
816 the program “Changing Earth – Sustaining our Future” of the Helmholtz Association. The campaign was partly
817 funded by the Institute for Advanced Study, Technical University of Munich (Grant no. 291763). The TUM
818 authors are partly supported by ERC Consolidator Grant CoSense4Climate (Grant 101089203) and Bavarian State
819 Ministry of the Environment (Grant TLK 01U-75487). [Yaowei Li acknowledges partial support from the NOAA](#)
820 [Climate and Global Change Postdoctoral Fellowship Program, administered by UCAR's Cooperative Programs](#)
821 [for the Advancement of Earth System Science \(CPAESS\) under award #NA23OAR4310383B.](#)

822 **5. References**

- 823 Ahn, J.-W., Dinh, T.-V., Park, S.-Y., Choi, I.-Y., Park, C.-R., and Son, Y.-S.: Characteristics of biogenic volatile
824 organic compounds emitted from major species of street trees and urban forests, *Atmospheric Pollution*
825 *Research*, 13, 10.1016/j.apr.2022.101470, 2022.
- 826 Äijälä, M., Daellenbach, K. R., Canonaco, F., Heikkinen, L., Junninen, H., Petäjä, T., Kulmala, M., Prévôt, A. S.
827 H., and Ehn, M.: Constructing a data-driven receptor model for organic and inorganic aerosol – a synthesis
828 analysis of eight mass spectrometric data sets from a boreal forest site, *Atmos. Chem. Phys.*, 19, 3645-3672,
829 10.5194/acp-19-3645-2019, 2019.
- 830 Äijälä, M., Heikkinen, L., Fröhlich, R., Canonaco, F., Prévôt, A. S. H., Junninen, H., Petäjä, T., Kulmala, M.,
831 Worsnop, D., and Ehn, M.: Resolving anthropogenic aerosol pollution types – deconvolution and exploratory

832 classification of pollution events, *Atmospheric Chemistry and Physics*, 17, 3165-3197, 10.5194/acp-17-3165-
833 2017, 2017.

834 Allison C. Aiken, Peter F. DeCarlo, Jesse H. Kroll, Douglas R. Worsnop, J. Alex Huffman, Kenneth S. Docherty,
835 Ingrid M. Ulbrich, Claudia Mohr, Joel R. Kimmel, Donna Sueper, Yele Sun, Qi Zhang, Achim Trimborn,
836 Megan Northway, Paul J. Ziemann, Manjula R. Canagaratna, Timothy B. Onasch, M. Rami Alfarra, and Prevot,
837 A. S. H.: O/C and OM/OC Ratios of Primary, Secondary, and Ambient Organic Aerosols with High-
838 Resolution Time-of-Flight Aerosol Mass Spectrometry, *Environmental Science & Technology*, 42, 4478-4485,
839 2008.

840 Messwertarchiv - LfU Bayern: <https://www.lfu.bayern.de/luft/immissionsmessungen/messwertarchiv/index.htm>,
841 last access: 29.09.

842 Belis, C. A., Larsen, B. R., Amato, F., El Haddad, I., Favez, O., Harrison, R. M., Hopke, P. K., Nava, S., Paatero,
843 P., Prévôt, A., Quass, U., Vecchi, R., and Viana, M.: European Guide on Air Pollution Source Apportionment
844 with Receptor Models, European Commission, Joint Research Centre, Institute for Environment and
845 Sustainability, Luxembourg: Publications Office of the European Union, 10.2788/9307, 2013.

846 Borbon, A., Herve, F., Marc, V., Nadine, L., J.C., G., and Renle, G.: An investigation into the traffic-related
847 fraction of isoprene at an urban location, *Atmospheric Environment*, 35, 3749–3760, 2001.

848 Bressi, M., Sciare, J., Gherzi, V., Bonnaire, N., Nicolas, J. B., Petit, J. E., Moukhtar, S., Rosso, A., Mihalopoulos,
849 N., and Féron, A.: A one-year comprehensive chemical characterisation of fine aerosol (PM_{2.5}) at urban,
850 suburban and rural background sites in the region of Paris (France), *Atmos. Chem. Phys.*, 13, 7825-7844,
851 10.5194/acp-13-7825-2013, 2013.

852 Bruns, E. A., Slowik, J. G., El Haddad, I., Kilic, D., Klein, F., Dommen, J., Temime-Roussel, B., Marchand, N.,
853 Baltensperger, U., and Prévôt, A. S. H.: Characterization of gas-phase organics using proton transfer reaction
854 time-of-flight mass spectrometry: fresh and aged residential wood combustion emissions, *Atmospheric
855 Chemistry and Physics*, 17, 705-720, 10.5194/acp-17-705-2017, 2017.

856 Canagaratna, M. R., Jimenez, J. L., Kroll, J. H., Chen, Q., Kessler, S. H., Massoli, P., Hildebrandt Ruiz, L., Fortner,
857 E., Williams, L. R., Wilson, K. R., Surratt, J. D., Donahue, N. M., Jayne, J. T., and Worsnop, D. R.: Elemental
858 ratio measurements of organic compounds using aerosol mass spectrometry: characterization, improved
859 calibration, and implications, *Atmospheric Chemistry and Physics*, 15, 253-272, 10.5194/acp-15-253-2015,
860 2015.

861 Canagaratna, M. R., Jayne, J. T., Jimenez, J. L., Allan, J. D., Alfarra, M. R., Zhang, Q., Onasch, T. B., Drewnick,
862 F., Coe, H., Middlebrook, A., Delia, A., Williams, L. R., Trimborn, A. M., Northway, M. J., DeCarlo, P. F.,
863 Kolb, C. E., Davidovits, P., and Worsnop, D. R.: Chemical and microphysical characterization of ambient
864 aerosols with the aerodyne aerosol mass spectrometer, *Mass Spectrom Rev*, 26, 185-222, 10.1002/mas.20115,
865 2007.

866 Chakraborty, A., Tripathi, S. N., and Gupta, T.: Effects of organic aerosol loading and fog processing on organic
867 aerosol volatility, *Journal of Aerosol Science*, 105, 73-83, 10.1016/j.jaerosci.2016.11.015, 2017.

868 Chen, G., Canonaco, F., Slowik, J. G., Daellenbach, K. R., Tobler, A., Petit, J. E., Favez, O., Stavroulas, I.,
869 Mihalopoulos, N., Gerasopoulos, E., El Haddad, I., Baltensperger, U., and Prevot, A. S. H.: Real-Time Source
870 Apportionment of Organic Aerosols in Three European Cities, *Environ Sci Technol*, 56, 15290-15297,
871 10.1021/acs.est.2c02509, 2022a.

872 Chen, G., Canonaco, F., Tobler, A., Aas, W., Alastuey, A., Allan, J., Atabakhsh, S., Aurela, M., Baltensperger,
873 U., Bougiatioti, A., De Brito, J. F., Ceburnis, D., Chazeau, B., Chebaicheb, H., Daellenbach, K. R., Ehn, M.,
874 El Haddad, I., Eleftheriadis, K., Favez, O., Flentje, H., Font, A., Fossum, K., Freney, E., Gini, M., Green, D.
875 C., Heikkinen, L., Herrmann, H., Kalogridis, A. C., Keernik, H., Lhotka, R., Lin, C., Lunder, C., Maasikmets,
876 M., Manousakas, M. I., Marchand, N., Marin, C., Marmureanu, L., Mihalopoulos, N., Mocnik, G., Necki, J.,
877 O'Dowd, C., Ovadnevaite, J., Peter, T., Petit, J. E., Pikridas, M., Matthew Platt, S., Pokorna, P., Poulain, L.,
878 Priestman, M., Riffault, V., Rinaldi, M., Rozanski, K., Schwarz, J., Sciare, J., Simon, L., Skiba, A., Slowik, J.
879 G., Sosedova, Y., Stavroulas, I., Styszko, K., Teinmaa, E., Timonen, H., Tremper, A., Vasilescu, J., Via, M.,
880 Vodicka, P., Wiedensohler, A., Zografou, O., Cruz Minguillon, M., and Prevot, A. S. H.: European aerosol
881 phenomenology - 8: Harmonised source apportionment of organic aerosol using 22 Year-long ACSM/AMS
882 datasets, *Environ Int*, 166, 107325, 10.1016/j.envint.2022.107325, 2022b.

883 Dense Air Quality Sensor Network: <https://www.ee.cit.tum.de/esm/projekte/dense-air-quality-sensor-network>,
884 last access: 17 October.

885 Coggon, M. M., Stockwell, C. E., Xu, L., Peischl, J., Gilman, J. B., Lamplugh, A., Bowman, H. J., Aikin, K.,
886 Harkins, C., Zhu, Q., Schwantes, R. H., He, J., Li, M., Seltzer, K., McDonald, B., and Warneke, C.:
887 Contribution of cooking emissions to the urban volatile organic compounds in Las Vegas, NV, *Atmospheric
888 Chemistry and Physics*, 24, 4289-4304, 10.5194/acp-24-4289-2024, 2024a.

889 Coggon, M. M., Stockwell, C. E., Clafflin, M. S., Pfannerstill, E. Y., Xu, L., Gilman, J. B., Marcantonio, J., Cao,
890 C., Bates, K., Gkatzelis, G. I., Lamplugh, A., Katz, E. F., Arata, C., Apel, E. C., Hornbrook, R. S., Piel, F.,
891 Majluf, F., Blake, D. R., Wisthaler, A., Canagaratna, M., Lerner, B. M., Goldstein, A. H., Mak, J. E., and
892 Warneke, C.: Identifying and correcting interferences to PTR-ToF-MS measurements of isoprene and other
893 urban volatile organic compounds, *Atmos. Meas. Tech.*, 17, 801-825, 10.5194/amt-17-801-2024, 2024b.

894 Crippa, M., DeCarlo, P. F., Slowik, J. G., Mohr, C., Heringa, M. F., Chirico, R., Poulain, L., Freutel, F., Sciare,
895 J., Cozic, J., Di Marco, C. F., Elsasser, M., Nicolas, J. B., Marchand, N., Abidi, E., Wiedensohler, A.,
896 Drewnick, F., Schneider, J., Borrmann, S., Nemitz, E., Zimmermann, R., Jaffrezo, J. L., Prévôt, A. S. H., and
897 Baltensperger, U.: Wintertime aerosol chemical composition and source apportionment of the organic fraction
898 in the metropolitan area of Paris, *Atmospheric Chemistry and Physics*, 13, 961-981, 10.5194/acp-13-961-2013,
899 2013.

900 Daellenbach, K. R., Kourtschev, I., Vogel, A. L., Bruns, E. A., Jiang, J., Petäjä, T., Jaffrezo, J.-L., Aksoyoglu, S.,
901 Kalberer, M., Baltensperger, U., El Haddad, I., and Prévôt, A. S. H.: Impact of anthropogenic and biogenic
902 sources on the seasonal variation in the molecular composition of urban organic aerosols: a field and laboratory
903 study using ultra-high-resolution mass spectrometry, *Atmospheric Chemistry and Physics*, 19, 5973-5991,
904 10.5194/acp-19-5973-2019, 2019.

905 Debevec, C., Sauvage, S., Gros, V., Salameh, T., Sciare, J., Dulac, F., and Locoge, N.: Seasonal variation and
906 origins of volatile organic compounds observed during 2 years at a western Mediterranean remote background
907 site (Ersa, Cape Corsica), *Atmospheric Chemistry and Physics*, 21, 1449-1484, 10.5194/acp-21-1449-2021,
908 2021.

909 Docherty, K. S., Aiken, A. C., Huffman, J. A., Ulbrich, I. M., DeCarlo, P. F., Sueper, D., Worsnop, D. R., Snyder,
910 D. C., Peltier, R. E., Weber, R. J., Grover, B. D., Eatough, D. J., Williams, B. J., Goldstein, A. H., Ziemann,
911 P. J., and Jimenez, J. L.: The 2005 Study of Organic Aerosols at Riverside (SOAR-1): instrumental

912 intercomparisons and fine particle composition, *Atmospheric Chemistry and Physics*, 11, 12387-12420,
913 10.5194/acp-11-12387-2011, 2011.

914 Eichler, P., Müller, M., D'Anna, B., and Wisthaler, A.: A novel inlet system for online chemical analysis of semi-
915 volatile submicron particulate matter, *Atmospheric Measurement Techniques*, 8, 1353-1360, 10.5194/amt-8-
916 1353-2015, 2015.

917 Elser, M., Huang, R.-J., Wolf, R., Slowik, J. G., Wang, Q., Canonaco, F., Li, G., Bozzetti, C., Daellenbach, K. R.,
918 Huang, Y., Zhang, R., Li, Z., Cao, J., Baltensperger, U., El-Haddad, I., and Prévôt, A. S. H.: New insights into
919 PM_{2.5} chemical composition and sources in two major cities in China during extreme haze events using
920 aerosol mass spectrometry, *Atmospheric Chemistry and Physics*, 16, 3207-3225, 10.5194/acp-16-3207-2016,
921 2016.

922 Fleming, L. T., Lin, P., Roberts, J. M., Selimovic, V., Yokelson, R., Laskin, J., Laskin, A., and Nizkorodov, S.
923 A.: Molecular composition and photochemical lifetimes of brown carbon chromophores in biomass burning
924 organic aerosol, *Atmospheric Chemistry and Physics*, 20, 1105-1129, 10.5194/acp-20-1105-2020, 2020.

925 Freney, E. J., Sellegri, K., Canonaco, F., Boulon, J., Hervo, M., Weigel, R., Pichon, J. M., Colomb, A., Prévôt, A.
926 S. H., and Laj, P.: Seasonal variations in aerosol particle composition at the puy-de-Dôme research station in
927 France, *Atmospheric Chemistry and Physics*, 11, 13047-13059, 10.5194/acp-11-13047-2011, 2011.

928 Gkatzelis, G. I., Coggon, M. M., McDonald, B. C., Peischl, J., Gilman, J. B., Aikin, K. C., Robinson, M. A.,
929 Canonaco, F., Prevot, A. S. H., Trainer, M., and Warneke, C.: Observations Confirm that Volatile Chemical
930 Products Are a Major Source of Petrochemical Emissions in U.S. Cities, *Environ Sci Technol*, 55, 4332-4343,
931 10.1021/acs.est.0c05471, 2021.

932 Gkatzelis, G. I., Tillmann, R., Hohaus, T., Müller, M., Eichler, P., Xu, K.-M., Schlag, P., Schmitt, S. H., Wegener,
933 R., Kaminski, M., Holzinger, R., Wisthaler, A., and Kiendler-Scharr, A.: Comparison of three aerosol
934 chemical characterization techniques utilizing PTR-ToF-MS: a study on freshly formed and aged biogenic
935 SOA, *Atmospheric Measurement Techniques*, 11, 1481-1500, 10.5194/amt-11-1481-2018, 2018a.

936 Gkatzelis, G. I., Hohaus, T., Tillmann, R., Gensch, I., Müller, M., Eichler, P., Xu, K.-M., Schlag, P., Schmitt, S.
937 H., Yu, Z., Wegener, R., Kaminski, M., Holzinger, R., Wisthaler, A., and Kiendler-Scharr, A.: Gas-to-particle
938 partitioning of major biogenic oxidation products: a study on freshly formed and aged biogenic SOA,
939 *Atmospheric Chemistry and Physics*, 18, 12969-12989, 10.5194/acp-18-12969-2018, 2018b.

940 Grange, S. K., Fischer, A., Zellweger, C., Alastuey, A., Querol, X., Jaffrezo, J.-L., Weber, S., Uzu, G., and Hueglin,
941 C.: Switzerland's PM₁₀ and PM_{2.5} environmental increments show the importance of non-exhaust emissions,
942 *Atmospheric Environment: X*, 12, 100145, <https://doi.org/10.1016/j.aeaoa.2021.100145>, 2021.

943 Gruber, R. P. and Kalamas, N.: Current Concepts towards the Health Hazards of BBQ Smoke and Newer
944 Possibilities for Risk Mitigation: A Pilot Study, *Journal of Biomedical Research & Environmental Sciences*,
945 5, 675-682, 10.37871/jbres1942, 2024.

946 Guo, J., Zhang, J., Shao, J., Chen, T., Bai, K., Sun, Y., Li, N., Wu, J., Li, R., Li, J., Guo, Q., Cohen, J. B., Zhai,
947 P., Xu, X., and Hu, F.: A merged continental planetary boundary layer height dataset based on high-resolution
948 radiosonde measurements, ERA5 reanalysis, and GLDAS, *Earth Syst. Sci. Data*, 16, 1-14, 10.5194/essd-16-
949 1-2024, 2024.

950 Huang, D. D., Zhu, S., An, J., Wang, Q., Qiao, L., Zhou, M., He, X., Ma, Y., Sun, Y., Huang, C., Yu, J. Z., and
951 Zhang, Q.: Comparative Assessment of Cooking Emission Contributions to Urban Organic Aerosol Using

952 Online Molecular Tracers and Aerosol Mass Spectrometry Measurements, *Environ Sci Technol*, 55, 14526-
953 14535, 10.1021/acs.est.1c03280, 2021.

954 Huang, W., Saathoff, H., Shen, X., Ramisetty, R., Leisner, T., and Mohr, C.: Seasonal characteristics of organic
955 aerosol chemical composition and volatility in Stuttgart, Germany, *Atmospheric Chemistry and Physics*, 19,
956 11687-11700, 10.5194/acp-19-11687-2019, 2019.

957 Huang, X.-F., Zou, B.-B., He, L.-Y., Hu, M., Prévôt, A. S. H., and Zhang, Y.-H.: Exploration of PM_{2.5} sources on
958 the regional scale in the Pearl River Delta based on ME-2 modeling, *Atmospheric Chemistry and Physics*, 18,
959 11563-11580, 10.5194/acp-18-11563-2018, 2018.

960 IPCC: Climate Change 2023: Synthesis Report. Contribution of Working Groups I, II and III to the Sixth
961 Assessment Report of the Intergovernmental Panel on Climate Change 2023.

962 J. L. Jimenez, M. R. Canagaratna, N. M. Donahue, A. S. H. Prevot, Q. Zhang, J. H. Kroll, P. F. DeCarlo, J. D.
963 Allan, H. Coe, N. L. Ng, A. C. Aiken, K. S. Docherty, I. M. Ulbrich, and Grieshop, A. P.: Evolution of organic
964 aerosols in the atmosphere, *Science*, 326, 1525-1529, DOI: 10.1126/science.1180353, 2009.

965 Jain, V., Tripathi, S. N., Tripathi, N., Sahu, L. K., Gaddamidi, S., Shukla, A. K., Bhattu, D., and Ganguly, D.:
966 Seasonal variability and source apportionment of non-methane VOCs using PTR-TOF-MS measurements in
967 Delhi, India, *Atmospheric Environment*, 283, 10.1016/j.atmosenv.2022.119163, 2022.

968 Kabir, E., Kim, K. H., Ahn, J. W., Hong, O. F., and Sohn, J. R.: Barbecue charcoal combustion as a potential
969 source of aromatic volatile organic compounds and carbonyls, *J Hazard Mater*, 174, 492-499,
970 10.1016/j.jhazmat.2009.09.079, 2010.

971 Kajos, M. K., Rantala, P., Hill, M., Hellén, H., Aalto, J., Patokoski, J., Taipale, R., Hoerger, C. C., Reimann, S.,
972 and Ruuskanen, T. M.: Ambient measurements of aromatic and oxidized VOCs by PTR-MS and GC-MS:
973 intercomparison between four instruments in a boreal forest in Finland, *Atmospheric Measurement*
974 *Techniques*, 8, 4453-4473, 2015.

975 Kim, E., Hopke, P. K., Larson, T. V., Maykut, N. N., and Lewtas, J.: Factor Analysis of Seattle Fine Particles,
976 *Aerosol Science and Technology*, 38, 724-738, 10.1080/02786820490490119, 2004.

977 Kodros, J. K., Papanastasiou, D. K., Paglione, M., Masiol, M., Squizzato, S., Florou, K., Skyllakou, K.,
978 Kaltsonoudis, C., Nenes, A., and Pandis, S. N.: Rapid dark aging of biomass burning as an overlooked source
979 of oxidized organic aerosol, *Proc Natl Acad Sci U S A*, 117, 33028-33033, 10.1073/pnas.2010365117, 2020.

980 Koss, A. R., Sekimoto, K., Gilman, J. B., Selimovic, V., Coggon, M. M., Zarzana, K. J., Yuan, B., Lerner, B. M.,
981 Brown, S. S., Jimenez, J. L., Krechmer, J., Roberts, J. M., Warneke, C., Yokelson, R. J., and de Gouw, J.:
982 Non-methane organic gas emissions from biomass burning: identification, quantification, and emission factors
983 from PTR-ToF during the FIREX 2016 laboratory experiment, *Atmospheric Chemistry and Physics*, 18, 3299-
984 3319, 10.5194/acp-18-3299-2018, 2018.

985 Kourtchev, I., Godoi, R. H. M., Connors, S., Levine, J. G., Archibald, A. T., Godoi, A. F. L., Paralovo, S. L.,
986 Barbosa, C. G. G., Souza, R. A. F., Manzi, A. O., Seco, R., Sjostedt, S., Park, J.-H., Guenther, A., Kim, S.,
987 Smith, J., Martin, S. T., and Kalberer, M.: Molecular composition of organic aerosols in central Amazonia: an
988 ultra-high-resolution mass spectrometry study, *Atmospheric Chemistry and Physics*, 16, 11899-11913,
989 10.5194/acp-16-11899-2016, 2016.

990 Kumar, B., Chakraborty, A., Tripathi, S. N., and Bhattu, D.: Highly time resolved chemical characterization of
991 submicron organic aerosols at a polluted urban location, *Environ Sci Process Impacts*, 18, 1285-1296,
992 10.1039/c6em00392c, 2016.

993 Kumar, V., Giannoukos, S., Haslett, S. L., Tong, Y., Singh, A., Bertrand, A., Lee, C. P., Wang, D. S., Bhattu, D.,
994 Stefenelli, G., Dave, J. S., Puthussery, J. V., Qi, L., Vats, P., Rai, P., Casotto, R., Satish, R., Mishra, S.,
995 Pospisilova, V., Mohr, C., Bell, D. M., Ganguly, D., Verma, V., Rastogi, N., Baltensperger, U., Tripathi, S.
996 N., Prévôt, A. S. H., and Slowik, J. G.: Highly time-resolved chemical speciation and source apportionment
997 of organic aerosol components in Delhi, India, using extractive electrospray ionization mass spectrometry,
998 *Atmospheric Chemistry and Physics*, 22, 7739-7761, 10.5194/acp-22-7739-2022, 2022.

999 Lalchandani, V., Kumar, V., Tobler, A., M. Thamban, N., Mishra, S., Slowik, J. G., Bhattu, D., Rai, P., Satish,
1000 R., Ganguly, D., Tiwari, S., Rastogi, N., Tiwari, S., Močnik, G., Prévôt, A. S. H., and Tripathi, S. N.: Real-
1001 time characterization and source apportionment of fine particulate matter in the Delhi megacity area during
1002 late winter, *Science of The Total Environment*, 770, 10.1016/j.scitotenv.2021.145324, 2021.

1003 Lannuque, V., D'Anna, B., Kostenidou, E., Couvidat, F., Martinez-Valiente, A., Eichler, P., Wisthaler, A., Müller,
1004 M., Temime-Roussel, B., Valorso, R., and Sartelet, K.: Gas-particle partitioning of toluene oxidation products:
1005 an experimental and modeling study, *Atmospheric Chemistry and Physics*, 23, 15537-15560, 10.5194/acp-23-
1006 15537-2023, 2023.

1007 Leglise, J., Muller, M., Piel, F., Otto, T., and Wisthaler, A.: Bulk Organic Aerosol Analysis by Proton-Transfer-
1008 Reaction Mass Spectrometry: An Improved Methodology for the Determination of Total Organic Mass, O:C
1009 and H:C Elemental Ratios, and the Average Molecular Formula, *Anal Chem*, 91, 12619-12624,
1010 10.1021/acs.analchem.9b02949, 2019.

1011 Lemieux, P. M., Lutes, C. C., and Santoianni, D. A.: Emissions of organic air toxics from open burning: a
1012 comprehensive review, *Progress in Energy and Combustion Science*, 30, 1-32, 10.1016/j.peccs.2003.08.001,
1013 2004.

1014 Lenssen, E. S., Pieters, R. H. H., Nijmeijer, S. M., Oldenwening, M., Meliefste, K., and Hoek, G.: Short-term
1015 associations between barbecue fumes and respiratory health in young adults, *Environ Res*, 204, 111868,
1016 10.1016/j.envres.2021.111868, 2022.

1017 Li, H., Riva, M., Rantala, P., Heikkinen, L., Daellenbach, K., Krechmer, J. E., Flaud, P.-M., Worsnop, D., Kulmala,
1018 M., Villenave, E., Perraudin, E., Ehn, M., and Bianchi, F.: Terpenes and their oxidation products in the French
1019 Landes forest: insights from Vocus PTR-TOF measurements, *Atmospheric Chemistry and Physics*, 20, 1941-
1020 1959, 10.5194/acp-20-1941-2020, 2020a.

1021 Li, S., Liu, D., Wu, Y., Hu, K., Jiang, X., Tian, P., Sheng, J., Pan, B., and Zhao, D.: Aging effects on residential
1022 biomass burning emissions under quasi-real atmospheric conditions, *Environ Pollut*, 337, 122615,
1023 10.1016/j.envpol.2023.122615, 2023.

1024 Li, W., Wang, J., Qi, L., Yu, W., Nie, D., Shi, S., Gu, C., Ge, X., and Chen, M.: Molecular characterization of
1025 biomass burning tracer compounds in fine particles in Nanjing, China, *Atmospheric Environment*, 240,
1026 10.1016/j.atmosenv.2020.117837, 2020b.

1027 Liu, T., Wang, Z., Wang, X., and Chan, C. K.: Primary and secondary organic aerosol from heated cooking oil
1028 emissions, *Atmospheric Chemistry and Physics*, 18, 11363-11374, 10.5194/acp-18-11363-2018, 2018.

1029 Ma, J., Wang, S., Chen, G., Zhu, S., Wang, P., Chen, J., and Zhang, H.: Estimating emissions of biogenic volatile
1030 organic compounds from urban green spaces and their contributions to secondary pollution, *Environmental*
1031 *Science: Atmospheres*, 5, 129-141, 10.1039/d4ea00099d, 2025.

1032 Maison, A., Lugon, L., Park, S.-J., Baudic, A., Cantrell, C., Couvidat, F., D'Anna, B., Di Biagio, C., Gratien, A.,
1033 Gros, V., Kalalian, C., Kammer, J., Michoud, V., Petit, J.-E., Shahin, M., Simon, L., Valari, M., Vigneron, J.,
1034 Tuzet, A., and Sartelet, K.: Significant impact of urban tree biogenic emissions on air quality estimated by a
1035 bottom-up inventory and chemistry transport modeling, *Atmospheric Chemistry and Physics*, 24, 6011-6046,
1036 10.5194/acp-24-6011-2024, 2024.

1037 Malik, T. G., Sahu, L. K., Gupta, M., Mir, B. A., Gajbhiye, T., Dubey, R., Clavijo McCormick, A., and Pandey,
1038 S. K.: Environmental Factors Affecting Monoterpene Emissions from Terrestrial Vegetation, *Plants (Basel)*,
1039 12, 10.3390/plants12173146, 2023.

1040 Massoli, P., Stark, H., Canagaratna, M. R., Krechmer, J. E., Xu, L., Ng, N. L., Mauldin, R. L., Yan, C., Kimmel,
1041 J., Misztal, P. K., Jimenez, J. L., Jayne, J. T., and Worsnop, D. R.: Ambient Measurements of Highly Oxidized
1042 Gas-Phase Molecules during the Southern Oxidant and Aerosol Study (SOAS) 2013, *ACS Earth and Space*
1043 *Chemistry*, 2, 653-672, 10.1021/acsearthspacechem.8b00028, 2018.

1044 Middlebrook, A. M., Bahreini, R., Jimenez, J. L., and Canagaratna, M. R.: Evaluation of Composition-Dependent
1045 Collection Efficiencies for the Aerodyne Aerosol Mass Spectrometer using Field Data, *Aerosol Science and*
1046 *Technology*, 46, 258-271, 10.1080/02786826.2011.620041, 2012.

1047 Molteni, U., Bianchi, F., Klein, F., El Haddad, I., Frege, C., Rossi, M. J., Dommen, J., and Baltensperger, U.:
1048 Formation of highly oxygenated organic molecules from aromatic compounds, *Atmospheric Chemistry and*
1049 *Physics*, 18, 1909-1921, 10.5194/acp-18-1909-2018, 2018.

1050 Muller, M., Eichler, P., D'Anna, B., Tan, W., and Wisthaler, A.: Direct Sampling and Analysis of Atmospheric
1051 Particulate Organic Matter by Proton-Transfer-Reaction Mass Spectrometry, *Anal Chem*, 89, 10889-10897,
1052 10.1021/acs.analchem.7b02582, 2017.

1053 Müller, M., Mikoviny, T., Jud, W., D'Anna, B., and Wisthaler, A.: A new software tool for the analysis of high
1054 resolution PTR-TOF mass spectra, *Chemometrics and Intelligent Laboratory Systems*, 127, 158-165,
1055 10.1016/j.chemolab.2013.06.011, 2013.

1056 München, S.: LHM Stat. Faltkarte, [https://stadt.muenchen.de/dam/jcr%3AAddaedd0e-0914-4093-b46a-
1057 5a62acc9bf9/LHM-StatTB_2023_DS.pdf?utm_source=chatgpt.com](https://stadt.muenchen.de/dam/jcr%3AAddaedd0e-0914-4093-b46a-5a62acc9bf9/LHM-StatTB_2023_DS.pdf?utm_source=chatgpt.com), 2023.

1058 Nakao, S., Clark, C., Tang, P., Sato, K., and Cocker Iii, D.: Secondary organic aerosol formation from phenolic
1059 compounds in the absence of NO_x, *Atmospheric Chemistry and Physics*, 11, 10649-10660, 10.5194/acp-11-
1060 10649-2011, 2011.

1061 Nault, B. A., Jo, D. S., McDonald, B. C., Campuzano-Jost, P., Day, D. A., Hu, W., Schroder, J. C., Allan, J.,
1062 Blake, D. R., Canagaratna, M. R., Coe, H., Coggon, M. M., DeCarlo, P. F., Diskin, G. S., Dunmore, R., Flocke,
1063 F., Fried, A., Gilman, J. B., Gkatzelis, G., Hamilton, J. F., Hanisco, T. F., Hayes, P. L., Henze, D. K., Hodzic,
1064 A., Hopkins, J., Hu, M., Huey, L. G., Jobson, B. T., Kuster, W. C., Lewis, A., Li, M., Liao, J., Nawaz, M. O.,
1065 Pollack, I. B., Peischl, J., Rappenglück, B., Reeves, C. E., Richter, D., Roberts, J. M., Ryerson, T. B., Shao,
1066 M., Sommers, J. M., Walega, J., Warneke, C., Weibring, P., Wolfe, G. M., Young, D. E., Yuan, B., Zhang,
1067 Q., de Gouw, J. A., and Jimenez, J. L.: Secondary organic aerosols from anthropogenic volatile organic

1068 compounds contribute substantially to air pollution mortality, *Atmospheric Chemistry and Physics*, 21, 11201-
1069 11224, 10.5194/acp-21-11201-2021, 2021.

1070 Niu, Y., Yan, Y., Li, J., Liu, P., Liu, Z., Hu, D., Peng, L., and Wu, J.: Establishment and verification of
1071 anthropogenic volatile organic compound emission inventory in a typical coal resource-based city, *Environ*
1072 *Pollut*, 288, 117794, 10.1016/j.envpol.2021.117794, 2021.

1073 Ortega, A. M., Day, D. A., Cubison, M. J., Brune, W. H., Bon, D., de Gouw, J. A., and Jimenez, J. L.: Secondary
1074 organic aerosol formation and primary organic aerosol oxidation from biomass-burning smoke in a flow
1075 reactor during FLAME-3, *Atmospheric Chemistry and Physics*, 13, 11551-11571, 10.5194/acp-13-11551-
1076 2013, 2013.

1077 Paatero, P.: The Multilinear Engine—A Table-Driven, Least Squares Program for Solving Multilinear Problems,
1078 Including then-Way Parallel Factor Analysis Model, *Journal of Computational and Graphical Statistics*, 8,
1079 854-888, 10.1080/10618600.1999.10474853, 1999.

1080 Paatero, P. and Tapper, U.: Positive matrix factorization: A non-negative factor model with optimal utilization of
1081 error estimates of data values, *Environmetrics*, 5, 111-126, 10.1002/env.3170050203, 1994.

1082 Peron, A., Graus, M., Striednig, M., Lamprecht, C., Wohlfahrt, G., and Karl, T.: Deciphering anthropogenic and
1083 biogenic contributions to selected non-methane volatile organic compound emissions in an urban area,
1084 *Atmospheric Chemistry and Physics*, 24, 7063-7083, 10.5194/acp-24-7063-2024, 2024.

1085 Peter F. DeCarlo, Joel R. Kimmel, Achim Trimborn, Megan J. Northway, John T. Jayne, Allison C. Aiken, Marc
1086 Gonin, Katrin Fuhrer, Thomas Horvath, Kenneth S. Docherty, Doug R. Worsnop, and Jimenez, J. L.: Field-
1087 Deployable, High-Resolution, Time-of-Flight Aerosol Mass Spectrometer, *Analytical Chemistry*, 78, 8281-
1088 8289, 10.1029/2001jd001213, 2006.

1089 Pfannerstill, E. Y., Wang, N., Edtbauer, A., Bourtsoukidis, E., Crowley, J. N., Dienhart, D., Eger, P. G., Ernle, L.,
1090 Fischer, H., Hottmann, B., Paris, J.-D., Stöner, C., Tadic, I., Walter, D., Lelieveld, J., and Williams, J.:
1091 Shipborne measurements of total OH reactivity around the Arabian Peninsula and its role in ozone chemistry,
1092 *Atmospheric Chemistry and Physics*, 19, 11501-11523, 10.5194/acp-19-11501-2019, 2019.

1093 Philippe Dagaut, Zahraa Dbouk , Nesrine Belhadj , Maxence Lailliau , and Benoit, R.: On the combustion of
1094 terpenes biofuels, *ASME Turbo Expo 2024: Turbomachinery Technical Conference and Exposition*, London,
1095 United Kingdom, DOI: 10.1115/GT2024-121549, 2024.

1096 Piel, F., Müller, M., Mikoviny, T., Pusede, S. E., and Wisthaler, A.: Airborne measurements of particulate organic
1097 matter by proton-transfer-reaction mass spectrometry (PTR-MS): a pilot study, *Atmospheric Measurement*
1098 *Techniques*, 12, 5947-5958, 10.5194/amt-12-5947-2019, 2019.

1099 Pugliese, G., Piel, F., Trefz, P., Sulzer, P., Schubert, J. K., and Miekisch, W.: Effects of modular ion-funnel
1100 technology onto analysis of breath VOCs by means of real-time mass spectrometry, *Anal Bioanal Chem*, 412,
1101 7131-7140, 10.1007/s00216-020-02846-8, 2020.

1102 Qadir, R. M., Abbaszade, G., Schnelle-Kreis, J., Chow, J. C., and Zimmermann, R.: Concentrations and source
1103 contributions of particulate organic matter before and after implementation of a low emission zone in Munich,
1104 Germany, *Environ Pollut*, 175, 158-167, 10.1016/j.envpol.2013.01.002, 2013.

1105 Qi, L., Vogel, A. L., Esmaeilirad, S., Cao, L., Zheng, J., Jaffrezzo, J.-L., Fermo, P., Kasper-Giebl, A., Daellenbach,
1106 K. R., Chen, M., Ge, X., Baltensperger, U., Prévôt, A. S. H., and Slowik, J. G.: A 1-year characterization of
1107 organic aerosol composition and sources using an extractive electrospray ionization time-of-flight mass

1108 spectrometer (EESI-TOF), *Atmospheric Chemistry and Physics*, 20, 7875-7893, 10.5194/acp-20-7875-2020,
1109 2020.

1110 Reizer, M., Calzolari, G., Maciejewska, K., Orza, J. A. G., Carraresi, L., Lucarelli, F., and Juda-Rezler, K.:
1111 Measurement report: Receptor modeling for source identification of urban fine and coarse particulate matter
1112 using hourly elemental composition, *Atmos. Chem. Phys.*, 21, 14471-14492, 10.5194/acp-21-14471-2021,
1113 2021.

1114 Ren, Y., Ge, Y., Gu, B., Min, Y., Tani, A., and Chang, J.: Role of management strategies and environmental
1115 factors in determining the emissions of biogenic volatile organic compounds from urban greenspaces, *Environ*
1116 *Sci Technol*, 48, 6237-6246, 10.1021/es4054434, 2014.

1117 Renard, J.-B., Becker, G., Nodorft, M., Tavakoli, E., Thiele, L., Poincelet, E., Scholz, M., and Surcin, J.: High-
1118 Spatial Resolution Maps of PM_{2.5} Using Mobile Sensors on Buses: A Case Study of Teltow City, Germany,
1119 in the Suburb of Berlin, 2023, 10.3390/atmos15121494, 2024.

1120 Resler, J., Baueroová, P., Belda, M., Bureš, M., Eben, K., Fuka, V., Geletič, J., Jareš, R., Karel, J., Keder, J., Krč,
1121 P., Patiño, W., Radović, J., Řezníček, H., Sühning, M., Šindelářová, A., and Vlček, O.: Challenges of high-
1122 fidelity air quality modeling in urban environments – PALM sensitivity study during stable conditions,
1123 *Geoscientific Model Development*, 17, 7513-7537, 10.5194/gmd-17-7513-2024, 2024.

1124 Reyes-Villegas, E., Green, D. C., Priestman, M., Canonaco, F., Coe, H., Prévôt, A. S. H., and Allan, J. D.: Organic
1125 aerosol source apportionment in London 2013 with ME-2: exploring the solution space with annual and
1126 seasonal analysis, *Atmospheric Chemistry and Physics*, 16, 15545-15559, 10.5194/acp-16-15545-2016, 2016.

1127 Reyes-Villegas, E., Bannan, T., Le Breton, M., Mehra, A., Priestley, M., Percival, C., Coe, H., and Allan, J. D.:
1128 Online Chemical Characterization of Food-Cooking Organic Aerosols: Implications for Source
1129 Apportionment, *Environ Sci Technol*, 52, 5308-5318, 10.1021/acs.est.7b06278, 2018.

1130 Rios, J. C. R.: *Atmospheric Chemistry of Isoprene Hydroxyhydroperoxides*, The Department of Chemistry and
1131 Chemical Biology, Harvard University, 159 pp., 2018.

1132 Riva, M., Budisulistiorini, S. H., Chen, Y., Zhang, Z., D'Ambro, E. L., Zhang, X., Gold, A., Turpin, B. J., Thornton,
1133 J. A., Canagaratna, M. R., and Surratt, J. D.: Chemical Characterization of Secondary Organic Aerosol from
1134 Oxidation of Isoprene Hydroxyhydroperoxides, *Environ Sci Technol*, 50, 9889-9899,
1135 10.1021/acs.est.6b02511, 2016.

1136 Romanias, M. N., Coggon, M. M., Al Ali, F., Burkholder, J. B., Dagaut, P., Decker, Z., Warneke, C., Stockwell,
1137 C. E., Roberts, J. M., Tomas, A., Houzel, N., Coeur, C., and Brown, S. S.: Emissions and Atmospheric
1138 Chemistry of Furanoids from Biomass Burning: Insights from Laboratory to Atmospheric Observations, *ACS*
1139 *Earth and Space Chemistry*, 8, 857-899, 10.1021/acsearthspacechem.3c00226, 2024.

1140 Samad, A., Caballero Arciénega, N. A., Alabdallah, T., and Vogt, U.: Application of the Urban Climate Model
1141 PALM-4U to Investigate the Effects of the Diesel Traffic Ban on Air Quality in Stuttgart, *Atmosphere*, 15,
1142 10.3390/atmos15010111, 2024.

1143 Schäfer, K., Stefan, E., Stefanie, S., Szabina, T., Balint, A., Janos, O., Mike, P., Christoph, Munkel, Josef Cyrus,
1144 Annette Peters, and Sarigiannis, D.: A measurement based analysis of the spatial distribution, temporal
1145 variation and chemical composition of particulate matter in Munich and Augsburg, *Int J Tuberc Lung Dis*, 20,
1146 047-057, 10.5588/ijtld.10.0498, 2011.

1147 Schnell, F. I. J.: Aerosol distribution above Munich using remote sensing techniques, Dissertation LMU Munich,
1148 DOI: 10.5282/edoc.17368, 2014.

1149 Schnelle-Kreis J., Istvan Gebefügi, Gerhard Welzl, Thomas Jaensch, and Kettrup, A.: Occurrence of particle-
1150 associated polycyclic aromatic compounds in ambient air of the city of Munich, Atmospheric Environment,
1151 35, S71-S81, [https://doi.org/10.1016/S1352-2310\(00\)00557-4](https://doi.org/10.1016/S1352-2310(00)00557-4), 2001.

1152 Seidler, J., Friedrich, M. N., Thomas, C. K., and Nölscher, A. C.: Introducing the novel concept of cumulative
1153 concentration roses for studying the transport of ultrafine particles from an airport to adjacent residential areas,
1154 Atmospheric Chemistry and Physics, 24, 137-153, 10.5194/acp-24-137-2024, 2024.

1155 Setyan, A., Zhang, Q., Merkel, M., Knighton, W. B., Sun, Y., Song, C., Shilling, J. E., Onasch, T. B., Herndon,
1156 S. C., Worsnop, D. R., Fast, J. D., Zaveri, R. A., Berg, L. K., Wiedensohler, A., Flowers, B. A., Dubey, M. K.,
1157 and Subramanian, R.: Characterization of submicron particles influenced by mixed biogenic and
1158 anthropogenic emissions using high-resolution aerosol mass spectrometry: results from CARES, Atmospheric
1159 Chemistry and Physics, 12, 8131-8156, 10.5194/acp-12-8131-2012, 2012.

1160 Song, J., Saathoff, H., Jiang, F., Gao, L., Zhang, H., and Leisner, T.: Sources of organic gases and aerosol particles
1161 and their roles in nighttime particle growth at a rural forested site in southwest Germany, Atmospheric
1162 Chemistry and Physics, 24, 6699-6717, 10.5194/acp-24-6699-2024, 2024.

1163 Song, J., Saathoff, H., Gao, L., Gebhardt, R., Jiang, F., Vallon, M., Bauer, J., Norra, S., and Leisner, T.: Variations
1164 of PM_{2.5} sources in the context of meteorology and seasonality at an urban street canyon in Southwest
1165 Germany, Atmospheric Environment, 282, 10.1016/j.atmosenv.2022.119147, 2022.

1166 Squires, F. A., Nemitz, E., Langford, B., Wild, O., Drysdale, W. S., Acton, W. J. F., Fu, P., Grimmond, C. S. B.,
1167 Hamilton, J. F., Hewitt, C. N., Hollaway, M., Kotthaus, S., Lee, J., Metzger, S., Pingingtha-Durden, N., Shaw,
1168 M., Vaughan, A. R., Wang, X., Wu, R., Zhang, Q., and Zhang, Y.: Measurements of traffic-dominated
1169 pollutant emissions in a Chinese megacity, Atmospheric Chemistry and Physics, 20, 8737-8761, 10.5194/acp-
1170 20-8737-2020, 2020.

1171 Srivastava, D., Vu, T. V., Tong, S., Shi, Z., and Harrison, R. M.: Formation of secondary organic aerosols from
1172 anthropogenic precursors in laboratory studies, npj Climate and Atmospheric Science, 5, 10.1038/s41612-022-
1173 00238-6, 2022.

1174 Stein, A. F., Draxler, R. R., Rolph, G. D., Stunder, B. J. B., Cohen, M. D., and Ngan, F.: NOAA's HYSPLIT
1175 Atmospheric Transport and Dispersion Modeling System, Bulletin of the American Meteorological Society,
1176 96, 2059-2077, <https://doi.org/10.1175/BAMS-D-14-00110.1>, 2015.

1177 Stirnberg, R., Cermak, J., Kotthaus, S., Haeffelin, M., Andersen, H., Fuchs, J., Kim, M., Petit, J.-E., and Favez,
1178 O.: Meteorology-driven variability of air pollution (PM₁) revealed with explainable machine learning,
1179 Atmospheric Chemistry and Physics, 21, 3919-3948, 10.5194/acp-21-3919-2021, 2021.

1180 Ulbrich, I. M., Canagaratna, M. R., Zhang, Q., Worsnop, D. R., and Jimenez, J. L.: Interpretation of organic
1181 components from Positive Matrix Factorization of aerosol mass spectrometric data, Atmos. Chem. Phys., 9,
1182 2891-2918, 10.5194/acp-9-2891-2009, 2009.

1183 Vicente, E. D., Vicente, A., Evtyugina, M., Carvalho, R., Tarelho, L. A. C., Oduber, F. I., and Alves, C.:
1184 Particulate and gaseous emissions from charcoal combustion in barbecue grills, Fuel Processing Technology,
1185 176, 296-306, 10.1016/j.fuproc.2018.03.004, 2018.

1186 Wan, X., Kawamura, K., Ram, K., Kang, S., Loewen, M., Gao, S., Wu, G., Fu, P., Zhang, Y., Bhattarai, H., and
1187 Cong, Z.: Aromatic acids as biomass-burning tracers in atmospheric aerosols and ice cores: A review, *Environ*
1188 *Pollut*, 247, 216-228, 10.1016/j.envpol.2019.01.028, 2019.

1189 Wang, H., Li, Y., Liu, Y., Lu, X., Zhang, Y., Fan, Q., Shen, C., Lai, S., Zhou, Y., Zhang, T., and Yue, D.:
1190 Underappreciated contributions of biogenic volatile organic compounds from urban green spaces to ozone
1191 pollution, *Atmospheric Chemistry and Physics*, 25, 5233-5250, 10.5194/acp-25-5233-2025, 2025.

1192 Wang, L., Slowik, J. G., Tripathi, N., Bhattu, D., Rai, P., Kumar, V., Vats, P., Satish, R., Baltensperger, U.,
1193 Ganguly, D., Rastogi, N., Sahu, L. K., Tripathi, S. N., and Prévôt, A. S. H.: Source characterization of volatile
1194 organic compounds measured by proton-transfer-reaction time-of-flight mass spectrometers in Delhi, India,
1195 *Atmospheric Chemistry and Physics*, 20, 9753-9770, 10.5194/acp-20-9753-2020, 2020a.

1196 Wang, Q., He, X., Zhou, M., Huang, D. D., Qiao, L., Zhu, S., Ma, Y.-g., Wang, H.-l., Li, L., Huang, C., Huang,
1197 X. H. H., Xu, W., Worsnop, D., Goldstein, A. H., Guo, H., and Yu, J. Z.: Hourly Measurements of Organic
1198 Molecular Markers in Urban Shanghai, China: Primary Organic Aerosol Source Identification and
1199 Observation of Cooking Aerosol Aging, *ACS Earth and Space Chemistry*, 4, 1670-1685,
1200 10.1021/acsearthspacechem.0c00205, 2020b.

1201 Wang, W., Zhang, Y., Jiang, B., Chen, Y., Song, Y., Tang, Y., Dong, C., and Cai, Z.: Molecular characterization
1202 of organic aerosols in Taiyuan, China: Seasonal variation and source identification, *Sci Total Environ*, 800,
1203 149419, 10.1016/j.scitotenv.2021.149419, 2021.

1204 Wang, Z., Wang, Z., Sun, J., Wang, Y., Sun, Z., Ma, K., and Wei, L.: Investigation of oxygen-enriched atmosphere
1205 combustion of oily sludge: Performance, mechanism, emission of the S/N-containing compound, and residue
1206 characteristics, *Journal of Cleaner Production*, 378, 10.1016/j.jclepro.2022.134233, 2022.

1207 Wenzel, A., Chen, J., Klama, T., Böhm, F., Angleitner, M., and Lobmaier, R.: Towards high-resolution air
1208 pollutants sensing through dense low-cost sensor networks – a case study in Munich, EGU General Assembly
1209 2025, Vienna, Austria, 27 Apr–2 May 2025, <https://doi.org/10.5194/egusphere-egu25-16784>,

1210 Williams, L. R., Gonzalez, L. A., Peck, J., Trimborn, D., McInnis, J., Farrar, M. R., Moore, K. D., Jayne, J. T.,
1211 Robinson, W. A., Lewis, D. K., Onasch, T. B., Canagaratna, M. R., Trimborn, A., Timko, M. T., Magoon, G.,
1212 Deng, R., Tang, D., de la Rosa Blanco, E., Prévôt, A. S. H., Smith, K. A., and Worsnop, D. R.: Characterization
1213 of an aerodynamic lens for transmitting particles greater than 1 micrometer in diameter into the Aerodyne
1214 aerosol mass spectrometer, *Atmospheric Measurement Techniques*, 6, 3271-3280, 10.5194/amt-6-3271-2013,
1215 2013.

1216 The new 2021 WHO air quality guideline limits. Breeze Technologies Blog: [https://www.breeze-](https://www.breeze-technologies.de/blog/new-2021-who-air-quality-guideline-limits/)
1217 [technologies.de/blog/new-2021-who-air-quality-guideline-limits/](https://www.breeze-technologies.de/blog/new-2021-who-air-quality-guideline-limits/), last access: November 12.

1218 Wu, C., Wang, C., Wang, S., Wang, W., Yuan, B., Qi, J., Wang, B., Wang, H., Wang, C., Song, W., Wang, X.,
1219 Hu, W., Lou, S., Ye, C., Peng, Y., Wang, Z., Huangfu, Y., Xie, Y., Zhu, M., Zheng, J., Wang, X., Jiang, B.,
1220 Zhang, Z., and Shao, M.: Measurement report: Important contributions of oxygenated compounds to emissions
1221 and chemistry of volatile organic compounds in urban air, *Atmospheric Chemistry and Physics*, 20, 14769-
1222 14785, 10.5194/acp-20-14769-2020, 2020.

1223 Wu, T., Müller, T., Wang, N., Byron, J., Langer, S., Williams, J., and Licina, D.: Indoor Emission, Oxidation, and
1224 New Particle Formation of Personal Care Product Related Volatile Organic Compounds, *Environmental*
1225 *Science & Technology Letters*, 11, 1053-1061, 10.1021/acs.estlett.4c00353, 2024.

1226 Xu, C., Chen, J., Zhang, X., Cai, K., Chen, C., and Xu, B.: Emission characteristics and quantitative assessment
1227 of the health risks of cooking fumes during outdoor barbecuing, *Environ Pollut*, 323, 121319,
1228 10.1016/j.envpol.2023.121319, 2023.

1229 Ye, Q., Krechmer, J. E., Shutter, J. D., Barber, V. P., Li, Y., Helstrom, E., Franco, L. J., Cox, J. L., Hrdina, A. I.
1230 H., Goss, M. B., Tahsini, N., Canagaratna, M., Keutsch, F. N., and Kroll, J. H.: Real-Time Laboratory
1231 Measurements of VOC Emissions, Removal Rates, and Byproduct Formation from Consumer-Grade
1232 Oxidation-Based Air Cleaners, *Environmental Science & Technology Letters*, 8, 1020-1025,
1233 10.1021/acs.estlett.1c00773, 2021.

1234 Yee, L. D., Kautzman, K. E., Loza, C. L., Schilling, K. A., Coggon, M. M., Chhabra, P. S., Chan, M. N., Chan,
1235 A. W. H., Hersey, S. P., Crounse, J. D., Wennberg, P. O., Flagan, R. C., and Seinfeld, J. H.: Secondary organic
1236 aerosol formation from biomass burning intermediates: phenol and methoxyphenols, *Atmospheric Chemistry
1237 and Physics*, 13, 8019-8043, 10.5194/acp-13-8019-2013, 2013.

1238 Yeoman, A. M., Shaw, M., Carslaw, N., Murrells, T., Passant, N., and Lewis, A. C.: Simplified speciation and
1239 atmospheric volatile organic compound emission rates from non-aerosol personal care products, *Indoor Air*,
1240 30, 459-472, 10.1111/ina.12652, 2020.

1241 Zhang, H., Huang, W., Shen, X., Ramisetty, R., Song, J., Kiseleva, O., Holst, C. C., Khan, B., Leisner, T., and
1242 Saathoff, H.: Aerosol composition, air quality, and boundary layer dynamics in the urban background of
1243 Stuttgart in winter, *Atmospheric Chemistry and Physics*, 24, 10617-10637, 10.5194/acp-24-10617-2024, 2024.

1244 Zhang, Q., Jimenez JI Fau - Canagaratna, M. R., Canagaratna Mr Fau - Ulbrich, I. M., Ulbrich Im Fau - Ng, N.
1245 L., Ng NI Fau - Worsnop, D. R., Worsnop Dr Fau - Sun, Y., and Sun, Y.: Understanding atmospheric organic
1246 aerosols via factor analysis of aerosol mass spectrometry: a review, *Anal Bioanal Chem*, 401(10), 3045-3067,
1247 10.1007/s00216-011-5355-y, 2011.

1248 Zhu, Q., Huang, X.-F., Cao, L.-M., Wei, L.-T., Zhang, B., He, L.-Y., Elser, M., Canonaco, F., Slowik, J. G.,
1249 Bozzetti, C., El-Haddad, I., and Prévôt, A. S. H.: Improved source apportionment of organic aerosols in
1250 complex urban air pollution using the multilinear engine (ME-2), *Atmospheric Measurement Techniques*, 11,
1251 1049-1060, 10.5194/amt-11-1049-2018, 2018.

1252